



Changes in Extratropical Cyclone Precipitation and Associated Processes during the Twenty-First Century over Eastern North America and the Western Atlantic Using a Cyclone-Relative Approach

ZHENHAI ZHANG AND BRIAN A. COLLE

*School of Marine and Atmospheric Sciences, Stony Brook University, State University of New York,
Stony Brook, New York*

(Manuscript received 29 December 2016, in final form 21 July 2017)

ABSTRACT

This study investigates the future change in precipitation associated with extratropical cyclones over eastern North America and the western Atlantic during the cool season (November–March) through the twenty-first century. A cyclone-relative approach is applied to 10 models from phase 5 of the Coupled Model Intercomparison Project (CMIP5) in order to isolate precipitation changes for different cyclone intensities and storm life cycle, as well as determine the relevant physical processes associated with these changes. The historical analysis suggests that models with better performance in predicting extratropical cyclones tend to have smaller precipitation errors, and the ensemble mean has a smaller mean absolute error than the individual models. By the late-twenty-first century, the precipitation amount associated with cyclones increases by 5%–25% over the U.S. East Coast, with about 90% of the increase from the relatively strong (<990 hPa) and moderate (990–1005 hPa) cyclones. Meanwhile, the precipitation rate increases by 15%–25% over the U.S. East Coast for the strong cyclone centers, which is larger than the moderate and weak cyclones. The relatively strong cyclones just inland of the U.S. East Coast have the largest increase (~30%) in precipitation rate, since these centers over land have the largest increase in low-level temperature (and moisture), a decrease (5%–13%) in the static stability, and an increase (~5%) in upward motion during the late-twenty-first century. This east coast region also has an increase in cyclone intensity in the future even though there is a decrease in low-level baroclinicity, which suggests that the latent heat release from heavier precipitation contributes to this storm deepening.

1. Introduction

a. Background

Extratropical cyclones along the east coast of North America play an important role in the daily weather and regional climate. These cyclones contribute over 80% of the total cool-season precipitation over much of eastern North America (Hawcroft et al. 2012) and 93%–100% of extreme precipitation during the winter over the northeastern United States (Agel et al. 2015). They are also associated with inland flooding (Colle 2003), storm surge (Colle et al. 2008; Colle et al. 2015), and heavy snow (Novak et al. 2008; Picca et al. 2014), which have major environmental, economic, and societal impacts over this heavily populated region. Thus, it is important to understand how precipitation will change with extratropical

cyclones during the next several decades and the underlying mechanisms responsible for these changes.

The expected precipitation change from recent past decades into the later twenty-first century varies significantly in space and time. There is a decrease of precipitation in the subtropics and tropics outside of the monsoon trough through the twentieth century, while there is a large increase at mid- and high-latitude land areas, especially over North America and Eurasia (Trenberth 2011). In phase 5 of the Coupled Model Intercomparison Project (CMIP5; Taylor et al. 2012) simulations using the representative concentration pathway 8.5 scenario (RCP8.5), precipitation in the mid- and late-twenty-first century decreases over the Mediterranean Sea, Caribbean Sea, southwestern United States, and much of the subtropical

Corresponding author: Brian A. Colle, brian.colle@stonybrook.edu

Publisher's Note: This article was revised on 18 December 2018 to include the designation that it belongs to the Process-Oriented Model Diagnostics special collection.

DOI: 10.1175/JCLI-D-16-0906.1

© 2017 American Meteorological Society. For information regarding reuse of this content and general copyright information, consult the [AMS Copyright Policy](http://www.ametsoc.org/PUBSReuseLicenses) (www.ametsoc.org/PUBSReuseLicenses).

ocean, while it increases over the equatorial Pacific and Indian Oceans, with the largest percentage increase over the high-latitude continent during the cool season [IPCC Fifth Assessment Report (AR5); Knutti and Sedláček 2013; Chadwick et al. 2013; Lau et al. 2013]. Over eastern North America, the average precipitation amount increases $0.5\text{--}1.0\text{ mm day}^{-1}$ ($\sim 20\%$), with a high model agreement during 2070–99 winters (Maloney et al. 2014).

In a warming climate, water vapor is projected to increase with the temperature following the Clausius–Clapeyron (CC) relationship, resulting in an approximate 7% increase of water vapor for each 1 K of warming in the lower troposphere (Held and Soden 2006). However, the simulated global mean precipitation only increases by 1%–3% for each 1 K of global surface temperature warming because of the variations in the atmospheric circulation and energy balance (radiative forcing; Allen and Ingram 2002; Held and Soden 2006; Vecchi and Soden 2007; Stephens and Ellis 2008; O’Gorman et al. 2012), which in turn impacts the strength of the vertical motion and thermodynamic stability. Seager et al. (2010) demonstrated that under global warming the hydrological cycle [precipitation minus evaporation ($P - E$)] results in wet areas getting wetter (the ITCZ and mid-to-high latitudes) and dry areas getting drier (the subtropical dry zones). The wetter areas are enhanced by the specific humidity increase and offset to some extent by the slowdown of tropical circulation and expansion of the Hadley cell in the subtropics, while drying in the subtropics and precipitation increases at higher latitudes are amplified by the moisture transport by transient eddies (Seager et al. 2010).

The energy balance has a weaker constraint on the response of short-term heavy precipitation over high latitudes (Allan and Soden 2008). Increases in heavy precipitation are expected to be closer to the water vapor response of about $7\% \text{ K}^{-1}$ than the global-mean precipitation increase (Allen and Ingram 2002; Emori and Brown 2005). The future increase of heavy precipitation over many mid- and high-latitude continental regions in the Northern Hemisphere is larger than the mean increase (Scoccimarro et al. 2013), thus shifting the distribution of precipitation intensity toward heavier amounts. Maloney et al. (2014) found that most of the increased precipitation over eastern North America comes from more intense precipitation events. Lombardo et al. (2015) indicates a similar shift toward more frequent extreme precipitation events over the east coast of North America.

Many studies have shown a decrease in the number of the extratropical cyclones over North America and the North Atlantic (Chang 2013; Zappa et al. 2013; Colle et al. 2013). Meanwhile, increases in cyclone intensity

are found in some regional areas. Colle et al. (2013) found 10%–40% more intense ($<980\text{ hPa}$) cyclones and 20%–40% more rapid deepening rates just inland of the U.S. East Coast in the RCP8.5 experiments from selected CMIP5 models that perform best in simulating extratropical cyclones. Although there is a decrease in the total number of extratropical cyclones, there is no significant change in the number of wind speed extremes over the North Atlantic, and the precipitation associated with cyclones shows a shift toward heavier precipitation (Watterson 2006; Bengtsson et al. 2009; Zappa et al. 2013). Using a cyclone/noncyclone day approach for the 1979–2004 and 2009–98 cool seasons, Lombardo et al. (2015) illustrated that over the U.S. East Coast land there is a 12% increase in precipitation amount for all cyclone days, even though the number of cyclone days decreases through the twenty-first century, which was interpreted as a shift toward more frequent heavy precipitation events. Using high-resolution WRF simulations, Marciano et al. (2015) showed that the area-averaged precipitation around storm centers increases by about 33% in extratropical cyclones along the U.S. East Coast by the end of the twenty-first century.

b. Motivation

Several studies have indicated that precipitation will increase during the twenty-first century over the U.S. East Coast, but only a handful of studies (Marciano et al. 2015; Lombardo et al. 2015) have related these changes to extratropical cyclone changes over this region. Lombardo et al. (2015) investigated the future precipitation change during cyclone days, which were defined as days when a cyclone center was located within the U.S. East Coast domain. However, the spatial distribution of the precipitation change and the related physical processes within the cyclone system were not explored. This is best done using a cyclone-relative approach, but there have been limited studies using this approach to look at future changes in cyclones and precipitation. Marciano et al. (2015) used the pseudo-global warming (PGW) technique in their WRF future simulations to examine the future precipitation changes for extratropical cyclone cases using a cyclone-relative approach. Marciano et al. (2015) focused on 10 strongly developed “Miller-A” extratropical cyclones along the east coast. However, the future precipitation change for the other (weaker) cyclones is not clear.

Our study examines the future precipitation change due to extratropical cyclones during the twenty-first century, comparing the precipitation change for cyclones of different intensities and for different subregions over eastern North America and the western Atlantic. This study also explores the possible mechanisms for these

TABLE 1. The 10 CMIP5 models used in this study and their attributes. (Acronym expansions are available online at <http://www.ametsoc.org/PubsAcronymList>.)

Model	Center	Horizontal resolution (lon × lat)	No. of model levels	Reference
CCSM4	National Center for Atmospheric Research, United States	1.25° × 0.94°	26	Gent et al. (2011)
MRI-CGCM3	Meteorological Research Institute, Japan	1.125° × 1.12°	48	Yukimoto et al. (2012)
CNRM-CM5.1	Centre National de Recherches Météorologiques, France	1.4° × 1.4°	31	Michou et al. (2011)
HadGEM2-CC	Met Office Hadley Centre, United Kingdom (chemistry-coupled version)	1.875° × 1.25°	60	Jones et al. (2011)
INM-CM4.0	Institute of Numerical Mathematics, Russia	2.0° × 1.5°	21	Volodin et al. (2010)
IPSL-CM5A-MR	L'Institut Pierre-Simon Laplace, France	2.50° × 1.25°	39	Dufresne et al. (2013)
MPI-ESM-LR	Max Planck Institute for Meteorology, Germany	1.9° × 1.9°	47	Zanchettin et al. (2013)
GFDL-ESM2M	NOAA/Geophysical Fluid Dynamics Laboratory, United States	2.5° × 2.0°	24	Donner et al. (2011)
IPSL-CM5A-LR	L'Institut Pierre-Simon Laplace, France	3.75° × 1.8°	39	Dufresne et al. (2013)
MIROC-ESM-CHEM	Japan Agency for Marine-Earth Science and Technology, Japan	2.8° × 2.8°	80	Watanabe et al. (2011)

future precipitation changes. A cyclone-relative approach is employed to extract the precipitation associated with individual cyclone centers as well as the related fields impacting precipitation and cyclone development. In summary, this study will address the following questions:

- How will the cyclone-relative precipitation change over eastern North America and the western Atlantic through the twenty-first century?
- How will the precipitation change for the cyclone centers of different intensity and in different regions?
- Which physical processes are responsible for the precipitation changes in the region surrounding the cyclone?
- How will the cyclone-relative extreme precipitation change in relation to any changes in the cyclone intensity?

The data and methodology used in this study are described in [section 2](#). [Section 3](#) discusses the results of the cyclone-relative precipitation analyses. First, the model performance is evaluated in [section 3a](#). Then, the overall precipitation changes over eastern North America and the western Atlantic are explored in [section 3b](#). After that, the precipitation changes associated with cyclone centers in different subregions and of different intensity are compared in [section 3c](#), and the related physical processes are investigated in [section 3d](#). [Section 3e](#) provides a closer look at the future changes of precipitation extreme events. Conclusions and discussion are presented in [section 4](#).

2. Data and methods

For the historical (1979–2004) and future (2009–98) periods, 10 CMIP5 models ([Table 1](#)) were used. We chose these 10 models in order to maximize the overlap

with the 15 models used in [Colle et al. \(2013\)](#), although some models were not included because of their data availability. The future (RCP8.5) experiments were forced by enhanced greenhouse gas emissions, raising the radiative forcing pathway to 8.5 W m^{-2} by the end of the twenty-first century. Following [Colle et al. \(2013\)](#), we focused on the cool season from 1 November to 31 March and compared three future periods: early- (2009–38), mid- (2039–68), and late- (2069–98) twenty-first century. The historical period is used as a baseline to quantify the changes through the twenty-first century.

To evaluate the performance of those CMIP5 models in terms of precipitation, we compared the models' historical, seasonal-mean (1979–2004) precipitation with two monthly mean precipitation products at $2.5^\circ \times 2.5^\circ$ resolution, the Global Precipitation Climate Project (GPCP; [Adler et al. 2003](#)) and the Climate Prediction Center (CPC) Merged Analysis of Precipitation (CMAP; [Xie and Arkin 1997](#)). The GPCP data combined precipitation information available from several different sources, such as surface precipitation gauges and satellite. The CMAP data were obtained only from satellite estimates.

Following [Colle et al. \(2013\)](#), 6-hourly mean sea level pressure (MSLP) was used to track cyclones using the scheme developed by [Hodges \(1994, 1995\)](#), and only cyclones existing at least 24 h and moving at least 1000 km are retained for analysis. The minimum MSLP of the cyclone center was used as the index of cyclone intensity. The corresponding daily precipitation, air temperature, relative humidity, wind speed, and vertical motion (omega) at the surface and a few pressure levels were used to relate the precipitation changes to various physical processes. The 10 CMIP5 models have different

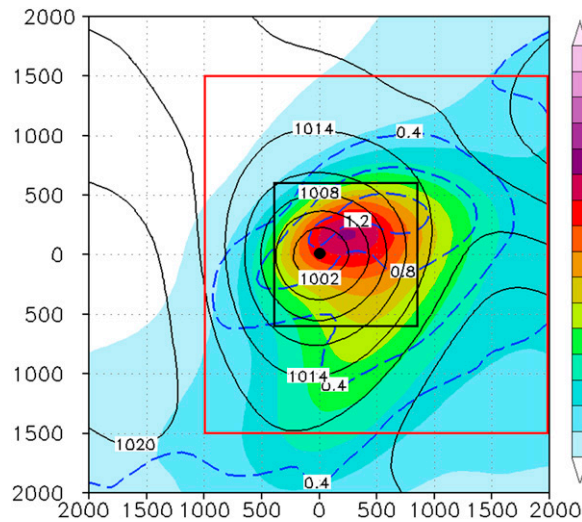


FIG. 1. The CMIP5 mean composite of cyclone-relative precipitation (colors; mm day^{-1}) and SLP (black contours; hPa) for the cyclone centers within ECL region during 1979–2004 cool seasons. The dashed blue contours are the spread (std dev; mm day^{-1}) of the models. The black dot is the cyclone center. The red box is the cyclone-relative box used to calculate the cyclone-relative precipitation over geophysical map. The small black box is used to calculate the mean precipitation for each cyclone center.

horizontal resolutions varying from $1.25^\circ \times 0.94^\circ$ to $2.8^\circ \times 2.8^\circ$. Thus, we first interpolate all model data to a common $1^\circ \times 1^\circ$ longitude–latitude grid.

A cyclone-relative approach is applied as in other studies (Chang and Song 2006; Field and Wood 2007; Naud et al. 2012, 2013; Marciano et al. 2015; Tamarin and Kaspi 2016). Using the cyclone data (the time, longitude, and latitude for each cyclone center), we first locate the cyclone center on the map and then define a $4000 \times 4000 \text{ km}^2$ cyclone-relative box around the cyclone center. The cyclone center is used as the origin for the new cyclone-relative x – y coordinate. A bilinear interpolation is utilized to convert the model data from the common geographic $1^\circ \times 1^\circ$ longitude–latitude grid to the cyclone-relative $100 \times 100 \text{ km}^2$ grid. The fields within the cyclone-relative box are stored for each storm, model, and time period. The cyclone-relative fields can be used to calculate the cyclone-related composite (average) fields on the cyclone coordinate, sharing the same cyclone center and overlapping the cyclone-relative fields. This composite approach can reproduce the amplitude and structure of the important fields around the cyclone center for a particular cyclone intensity category or over a particular region. Figure 1 shows the CMIP5 composite average of cyclone-relative precipitation and SLP for all cyclone centers passing within the ECL region during the historical (1979–2004)

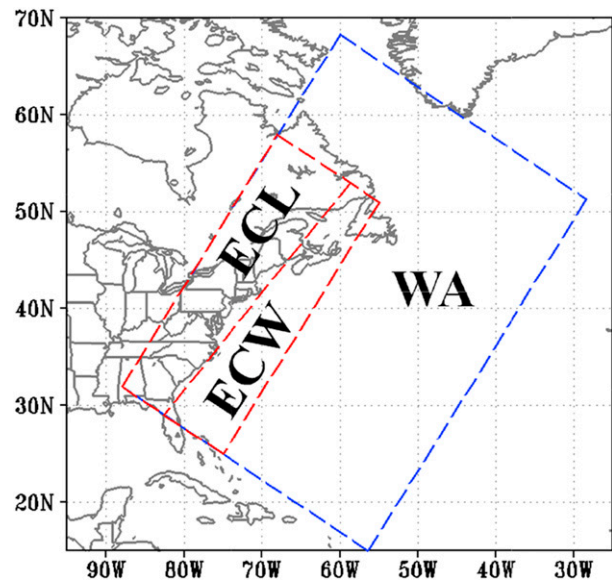


FIG. 2. The three domains used in this study: ECL, ECW, and WA.

cool seasons, in which the maximum precipitation is about 12.5 mm day^{-1} and the spread is 0.4 – 1.2 mm day^{-1} .

The cyclone-relative fields can be placed back onto the geographic map according to their original positions in order to create a geospatial-relative composite on the map, highlighting those relevant structures associated with cyclones. Since the cyclone data are 6-hourly (four cyclone centers at 0000, 0600, 1200, and 1800 UTC in each day), we converted the daily precipitation into four, equivalent, 6-hourly precipitation fields. Then we defined a $3000 \times 3000 \text{ km}^2$ cyclone-relative box (the red box in Fig. 1) for each cyclone center on the 6-hourly precipitation field. The precipitation within the cyclone-relative box was counted as cyclone-relative precipitation, and the sum of the cyclone-relative precipitation in a cool season was defined as the cyclone-relative precipitation amount of that cool season (mm season^{-1}). The cyclone-relative precipitation rate (mm day^{-1}) equals the cyclone-relative precipitation amount in a cool season divided by the cyclone frequency, which is the number of times a grid is covered by a cyclone-relative box in that cool season. The sensitivity of the results to the size of the cyclone-relative box was tested using a smaller box $2000 \times 2000 \text{ km}^2$, and the contribution of cyclone-relative precipitation to total amount decreases slightly (5%–17%), but there is no significant impact on our main conclusions regarding future changes.

In this study, cyclone centers were categorized based on the region and storm intensity. Following Colle et al. (2013), we used three regional domains over eastern North America and the western North Atlantic, as shown in Fig. 2: east coast land (ECL), east coast water

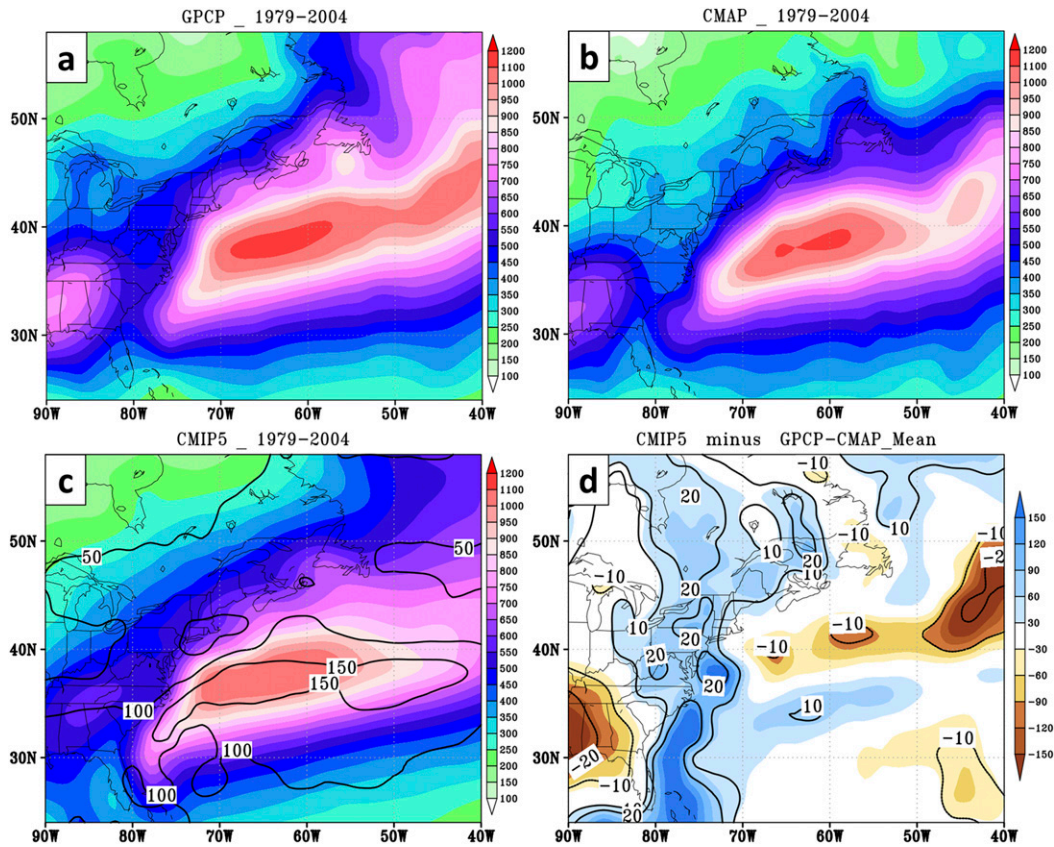


FIG. 3. The seasonal-mean precipitation amount (colors; mm season^{-1}) during 1979–2004 cool seasons for (a) GPCP, (b) CMAP, and (c) CMIP5 ensemble mean. The contours in (c) are the spread of the models (std dev; mm season^{-1}). (d) The difference in seasonal-mean precipitation (colors; mm season^{-1}) between the CMIP5 mean and the average of CMAP and GPCP (CMIP5 minus GPCP–CMAP) and the percentage of the difference (contours; %).

(ECW), and the western Atlantic (WA). The stronger cyclone centers tend to have larger precipitation rate since the precipitation rate is highly correlated with cyclone strength and available moisture (Field and Wood 2007; Pfahl and Sprenger 2016). Therefore, the cyclone centers were also categorized based on their intensity: strong (<990 hPa, S-Center), moderate (990–1005 hPa, M-Center), and weak center (>1005 hPa, W-Center) cyclones for the historical and future periods. Those thresholds were selected to make sure that we have enough cases for each category. For example, if we use <985 hPa to define the S-Center cyclone, in some models the sample size of S-Center cyclone within the ECL region will be too small, and the related future changes of precipitation may be dominated by a few extreme strong cases.

3. Results

a. Model evaluation

The performance of the 10 CMIP5 models used in this study was evaluated in terms of seasonal-mean

precipitation over eastern North America and the western Atlantic with respect to the average of the GPCP and CMAP precipitation (GPCP–CMAP). The seasonal precipitation amount for the ensemble mean of all models (CMIP5 mean) during the historical period has a maximum (over 1000 $\text{mm per cool season}$) over the east side of the western Atlantic storm track from 35° to 40°N , which is similar to GPCP and CMAP (Figs. 3a–c). The models have the largest spread of about 150 $\text{mm per cool season}$ near the precipitation maximum (Fig. 3c). Comparing with the GPCP–CMAP, the CMIP5 mean underestimates the precipitation amount by about 10% along the storm track and the precipitation amount by about 20% over the north side of the Gulf of Mexico (Fig. 3d). Meanwhile, the CMIP5 mean overestimates the precipitation over the U.S. East Coast, especially near the storm-track entrance region along the southeastern U.S. coast ($>20\%$). The individual models have larger bias than the ensemble mean. This is consistent with some other studies (Catto et al. 2010, 2015; Hawcroft et al. 2016) that suggest the climate models have limitations in

TABLE 2. The MAE and normalized MAE of historical (1979–2004) cool seasonal-mean precipitation amount over eastern North America and the western North Atlantic region (ECL + ECW + WA) with respect to the mean of GPCP and CMAP for individual CMIP5 models and the ensemble mean of CMIP5. The models in italics are the models that have relatively better performance in the cyclone simulation in Colle et al. (2013).

	Mean precipitation (mm season ⁻¹)	GPCP-CMAP MAE (mm season ⁻¹)	GPCP-CMAP normalized MAE (%)
GFDL-ESM2M	559.2	53.3	11.1
<i>CCSM4</i>	<i>547.0</i>	<i>71.0</i>	<i>13.7</i>
<i>CNRM-CM5</i>	<i>579.4</i>	<i>75.4</i>	<i>15.4</i>
<i>MPI-ESM-LR</i>	<i>550.8</i>	<i>85.8</i>	<i>18.5</i>
<i>MRI-CGCM3</i>	<i>546.7</i>	<i>82.9</i>	<i>18.9</i>
IPSL-CM5A-LR	510.7	93.1	19.0
MIROC-ESM-CHEM	540.8	103.4	19.6
INM-CM4.0	583.3	90.9	20.4
IPSL-CM5A-MR	517.5	106.6	22.3
<i>HadGEM2-CC</i>	<i>632.9</i>	<i>119.2</i>	<i>23.0</i>
CMIP5	557.3	48.2	9.5

simulating the precipitation associated with extratropical cyclones.

The performance of the individual models and the multimodel ensemble mean was quantified using GPCP-CMAP to obtain the mean absolute error (MAE; Table 2). The normalized MAE was calculated as well, normalized by GPCP-CMAP at each grid, describing the percentage error between the model and GPCP-CMAP. Lombardo et al. (2015) evaluated the cool-season precipitation in select CMIP5 models over the U.S. East Coast domain, which covers only a part of the storm track and precipitation maximum region. In our study, we quantified the model performance within a larger eastern North America and the western North Atlantic domain (ECL + ECW + WA), which covers the major part of the storm track as well as the precipitation maximum. The results provided an overall estimate of the precipitation error along the storm track over this region. The mean precipitation for this large domain is 540 mm per cool season for GPCP-CMAP. Our 10-member CMIP5 ensemble has smaller average error (MAE of ~ 48 mm per cool season and the normalized MAE of 9.5%) than each of the 10 models. Generally, the models with better cyclone historical predictions (CCSM4, CNRM-CM5, MPI-ESM-LR, and MRI-CGCM3), as obtained by Colle et al. (2013), tend to have smaller MAEs for the precipitation amount. However, there are exceptions, such as HadGEM2-CC, which has a relatively good cyclone performance but produces too much precipitation ($\sim 20\%$) along the storm track. The low-resolution ($2.0^\circ \times 2.5^\circ$) GFDL-ESM2M has the smallest MAE in precipitation amount, although it underestimates the cyclone frequency and intensity (Colle et al. 2013). We found that the cyclones in this model move slower ($\sim 42 \text{ km h}^{-1}$) than the other nine models

($\sim 49 \text{ km h}^{-1}$ for the mean of the 10 models); thus, more precipitation along each cyclone track likely compensates for the general cyclone underprediction. These results are different than Lombardo et al. (2015), who found that the precipitation performance of CMIP5 models in the east coast domain is less dependent on the performance of extratropical cyclone simulations. Their results may be more sensitive to the eastern boundary of their relatively small east coast domain, which is at the middle of storm track and the strong gradient of precipitation amount. Thus, a small shift of the storm track or the precipitation maximum may impact their results.

The individual models have large, normalized MAEs (11%–23%) over the large domain (ECL + ECW + WA), but the relatively small normalized MAE for the ensemble mean (9.5%) provides some confidence in examining the future precipitation changes.

b. Cyclone-relative precipitation over eastern North America and the western Atlantic

The overall future changes of cyclone-relative precipitation over eastern North America and the western Atlantic are explored in this section. The total cyclone-relative precipitation amount depends on two factors: the frequency of cyclones with precipitation impacting a given region and the precipitation rate for each cyclone center. Over eastern North America and the western North Atlantic, there are three center density maxima for the CMIP5 ensemble mean for all historical cyclones: around the Great Lakes, along the U.S. East Coast, and over the southeast of Greenland (Fig. 4a). Similar to the ensemble mean of the 15 CMIP5 models in Colle et al. (2013), the models reproduced the storm track successfully, but the mean track is shifted too close to the coast compared to the results of the Climate Forecast System

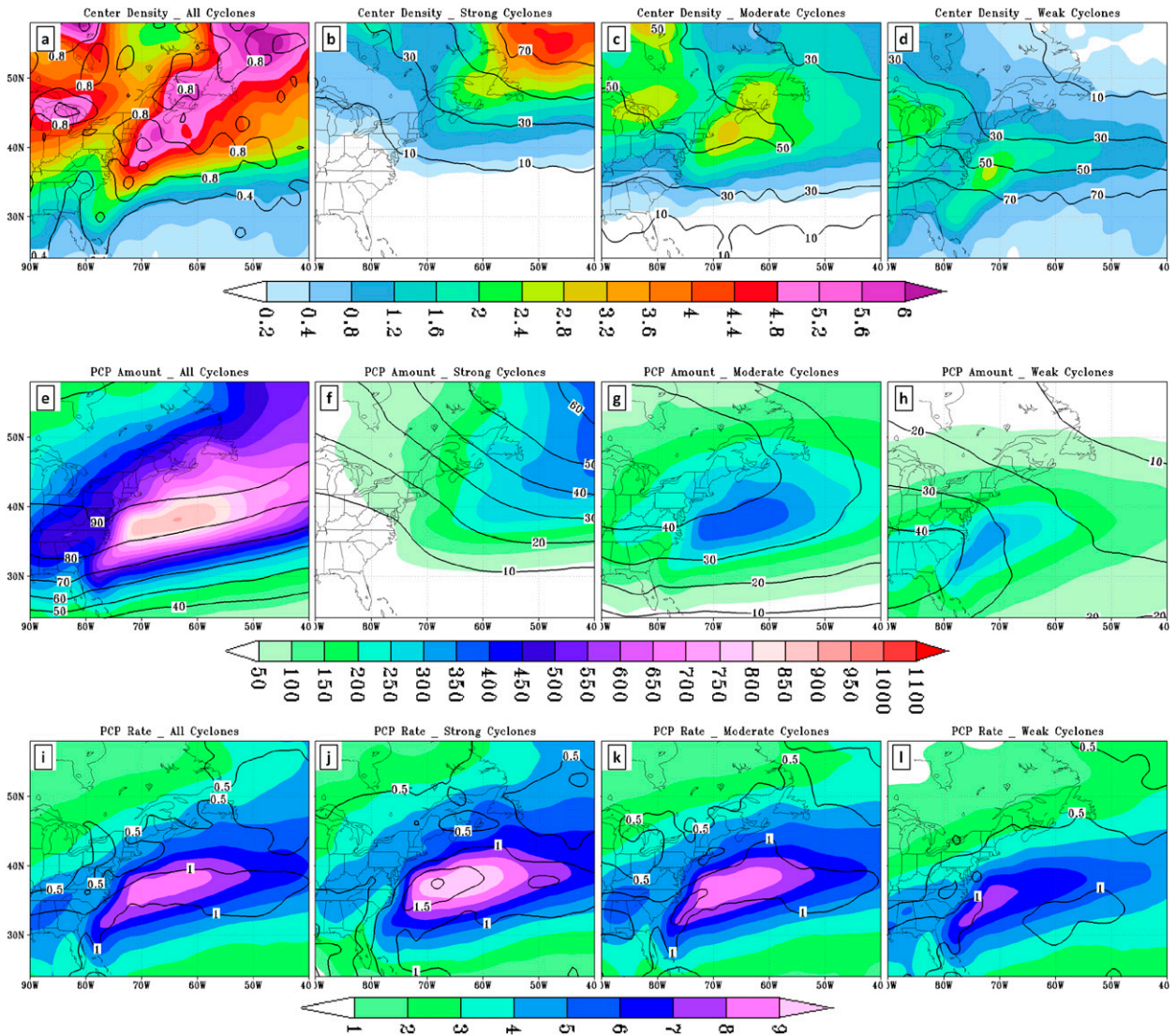


FIG. 4. (a)–(d) The historical (1979–2004) mean cyclone center density (colors; number of cyclone centers per 50 000 km² per cool season); the contours in (a) are the model spread, and the contours in (b)–(d) are the contribution (%) to the total density. (e)–(h) The historical-mean cyclone-relative precipitation amount (colors; mm season⁻¹) and the contribution (contours; %) to the total precipitation amount. (i)–(l) The historical-mean, cyclone-relative precipitation rate (colors; mm day⁻¹) and the model spread (contours; mm day⁻¹). (left)–(right) The results for all and S-, M-, and W-Center cyclones for the CMIP5 mean.

Reanalysis (CFRSR). The precipitation amount associated with those cyclone centers (the precipitation within the red box in Fig. 1) contributes from 50% to 60% at relatively lower latitude ($\sim 25^{\circ}\text{N}$) to over 90% at relatively higher latitude ($>40^{\circ}\text{N}$) to the total precipitation amount (contours in Fig. 4e), which is consistent with previous studies (Hawcroft et al. 2012; Agel et al. 2015). The cyclone-relative precipitation rate, which is normalized to each cyclone center, is maximized ($>8\text{ mm day}^{-1}$) over the western North Atlantic close to the coast between 33° and 40°N (Fig. 4i), with the largest standard deviation ($>1\text{ mm day}^{-1}$) over the same region. The

cyclone center density (Figs. 4b–d) and precipitation amount (Figs. 4f–h) for S-Center, M-Center, and W-Center cyclones have the largest values over high ($>50^{\circ}\text{N}$), middle (40° – 50°N), and low ($<40^{\circ}\text{N}$) latitudes, respectively. This distribution is likely the result of storms increasing in intensity as they move from southwest to northeast over the western Atlantic. The area of highest density for a W-Center cyclone is a climatologically favorable region for cyclogenesis given the presence of strong baroclinicity (e.g., Gulf Stream). In contrast with the precipitation amount, the cyclone-relative precipitation rate normalized for each cyclone

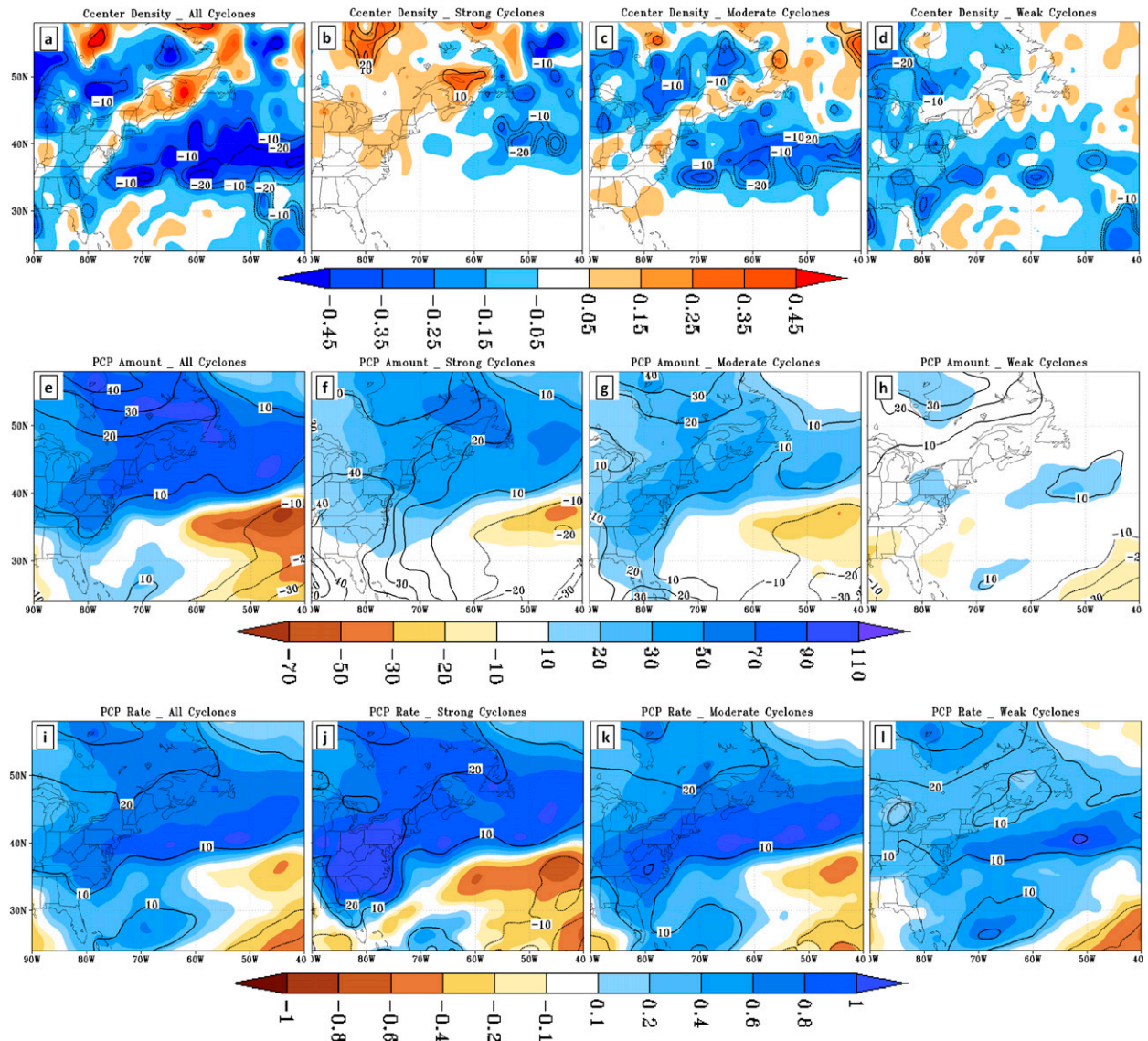


FIG. 5. As in Fig. 4, but for the future changes in late-twenty-first century (2069–98), and the contours are the percentage (%) of the changes.

center has a similar spatial distribution (maxima between 30° and 40°N) for S-Center, M-Center, and W-Center cyclones (Figs. 4j–l). The region along the Gulf Stream boundary has strong, low-level baroclinicity and moisture availability, which can enhance the rates as the cyclone develops.

The future change in cyclone density and cyclone-relative precipitation was calculated for three future cool seasons: 2009–38, 2039–68, and 2069–98. The precipitation change is most pronounced during the late-twenty-first century, and thus we only show and discuss the results for the later twenty-first century (Fig. 5). During the late-twenty-first century, there is a decrease

in cyclone center density over most areas of eastern North America and the western North Atlantic, and the largest decrease (10%–20%) is over the western North Atlantic (Fig. 5a). However, along the U.S. East Coast there is very little change or a slight increase (5%–10%) just inland of the coast (much of ECL region), as also shown in Colle et al. (2013). Most of this increase for the ECL originates from the S-Center and M-Center cyclones (Figs. 5a–d). Meanwhile, the normalized cyclone-relative precipitation rate increases by 10%–20% over the storm-track region (Figs. 5i–l). Over the U.S. East Coast region from the historical period to the late-twenty-first century, the precipitation rate of the S-Center cyclone

increases by 20%–30%, which is larger than the mean of all cyclone centers. The precipitation rate increase is smaller for the M-Center (10%–20%) and W-Center (around 10%) cyclones along the U.S. East Coast.

The cyclone-relative precipitation amount increases 5%–25% over the east coast of North America (Fig. 5e). The S-Center cyclone has a large increase (>30%) in precipitation amount over the east coast (Fig. 5f) because of the 20%–30% precipitation rate increase (Fig. 5j) and the slight increase in the frequency of S-Center cyclones (Fig. 5b). The M-Center cyclone also has an increase (10%–20%) in the precipitation amount over the east coast (Fig. 5g). However, the precipitation amount for the W-Center cyclone has little change along the east coast (Fig. 5h). Although the precipitation rate associated with W-Center cyclones increases slightly (~10%; Fig. 5l), the frequency of W-Center cyclone decreases over the coast (Fig. 5d). Overall, the relatively stronger cyclone centers have larger increases in both precipitation amount and precipitation rate over ECL region, and most of the increase in precipitation amount comes from the S-Center and M-Center cyclones.

The local extreme precipitation rate relative to the cyclone was also mapped back to the geographic map. At each grid point on the map, the precipitation rate values are recorded when that point is in a cyclone-relative box (associated with cyclone), and the precipitation rate is at least 1 mm day^{-1} (removing the noise of small value). Using this dataset, the precipitation extreme is defined using the 95th percentile for the historical and three future periods, respectively, for each model. Figure 6a shows the mean 95th threshold of the 10 CMIP5 models at each grid point for the historical period. There are two maxima (over 30 mm day^{-1}): one along the storm track and another to the north of the Gulf of Mexico. The frequency of extreme precipitation events along the U.S. East Coast is around 3 days per cool season. During the late-twenty-first century, the largest increase ($>5 \text{ mm day}^{-1}$, about 20%) is concentrated near the east coast (ECL and ECW), while the increase within the WA region is smaller (Fig. 6b). The results using the 99th percentile to define the extreme events are similar. This indicates that the largest increase in the precipitation extremes is just along the U.S. East Coast.

c. Future changes of precipitation for cyclone centers in different regions and intensity

The results in the previous section show that the relatively stronger cyclones have a larger increase in precipitation, and the increases over the ECL region are larger than the ECW and WA region. Hence, the different precipitation changes around cyclone centers in

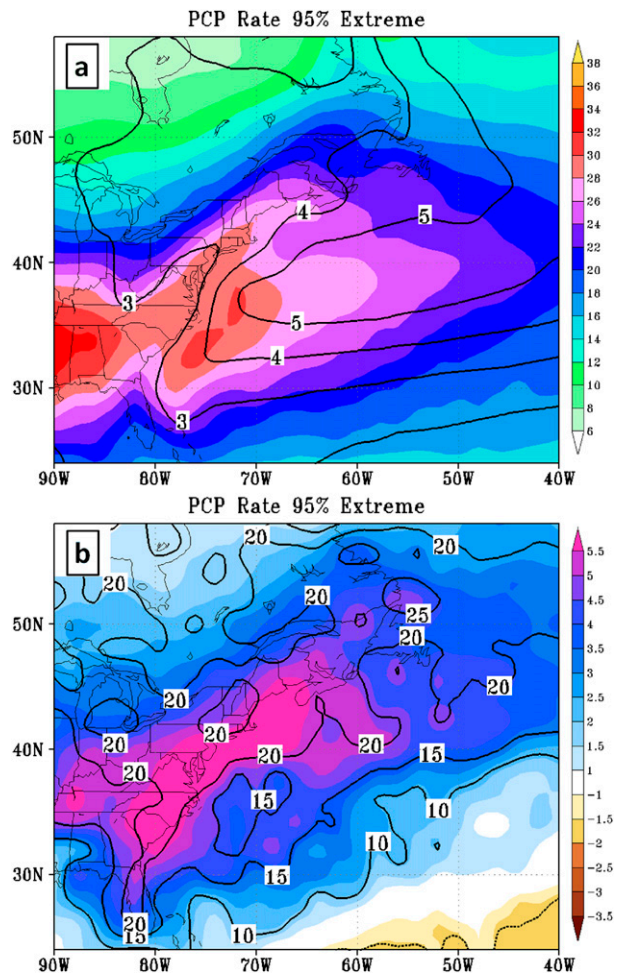


FIG. 6. (a) The cyclone-relative extreme (95th percentile) precipitation rate (colors; mm day^{-1}) and the frequency (contours; days per cool season) during historical cool seasons for the CMIP5 mean. (b) The future changes of the cyclone-relative extreme precipitation rate (colors; mm day^{-1}), and the contours are percentages.

different regions and of different intensity are compared in this section.

The composite precipitation shown relative to the cyclone center was calculated within ECL, ECW, and WA to explore the future change in precipitation for different environments. The historical maximum precipitation around the ECW cyclone center is the largest ($\sim 16 \text{ mm day}^{-1}$), while the WA has the smallest amounts ($\sim 10 \text{ mm day}^{-1}$), and the ECL region precipitation ($\sim 12 \text{ mm day}^{-1}$) is between the ECW and WA (Figs. 7a,c,e). The ECW centers that are near the Gulf Stream have the largest moisture content within the warm sector. Meanwhile, there is much less moisture content (20%–30% less at 850–250 hPa) for the WA centers offshore, since most of the WA cyclone centers

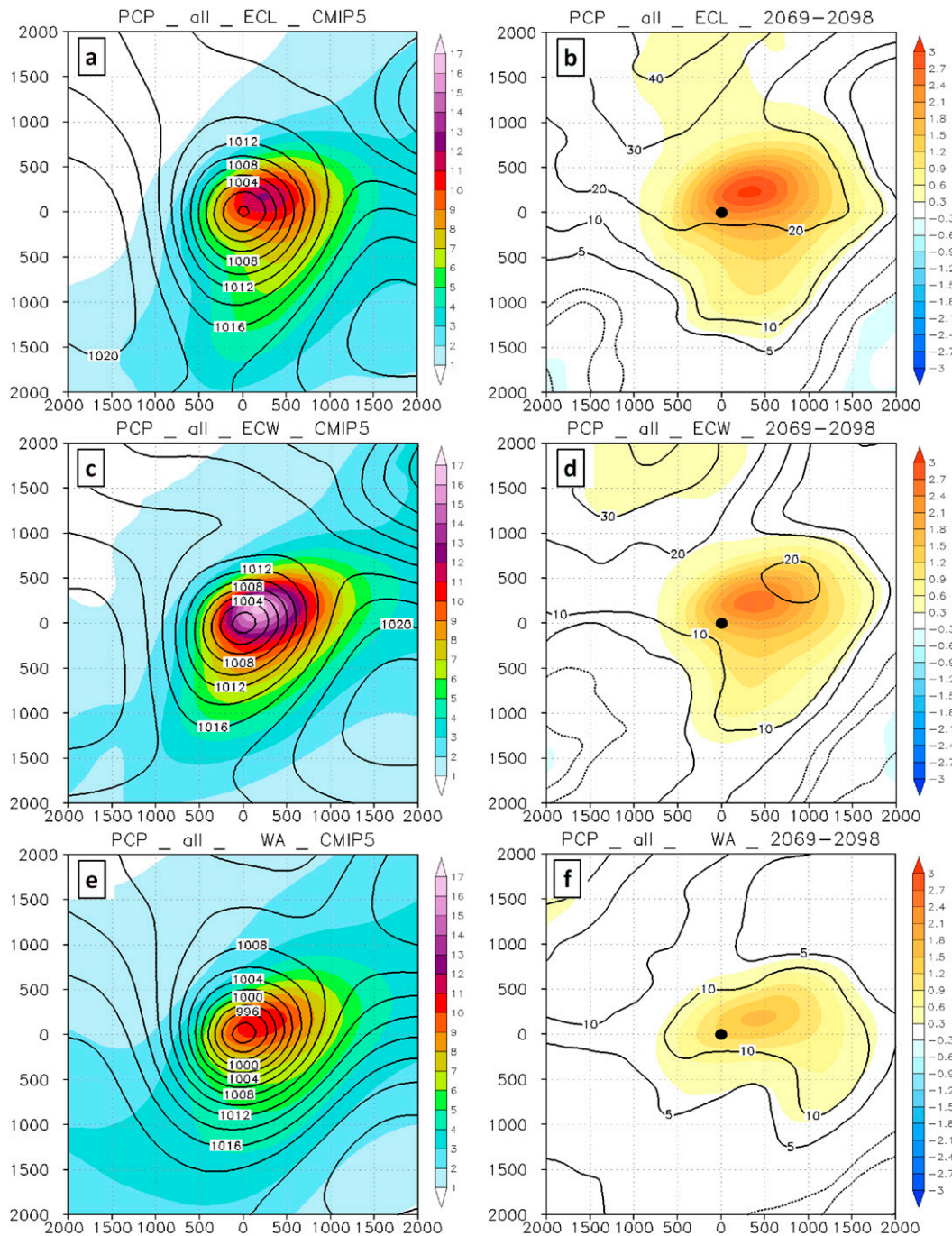


FIG. 7. (a),(c),(e) The composite cyclone for SLP (contours; every 2 hPa) and precipitation (colors; mm day^{-1}) around the cyclone (axes in km) during historical cool seasons for CMIP5 mean. (b),(d),(f) The future changes of precipitation (colors; mm day^{-1}) for late-twenty-first century seasons (2069–98 minus 1979–2004); the contours are the percentage changes. (top)–(bottom) The cyclone centers within ECL, ECW, and WA region.

are farther north over the relatively cool ocean. The difference in other factors (vertical motion, upper-level jet, and static stability) that impacts precipitation is less than the difference in moisture content for the ECL,

ECW, and WA cyclone centers. During the late-twenty-first century, the ECL cyclone centers have the largest increase in precipitation rate in terms of both the amount and percentage (Figs. 7b,d,f). The maximum increase

around ECL cyclone centers is just northeast of the storm center, about 3 mm day^{-1} ($>20\%$). It indicates that this increase is likely associated with warm frontal precipitation. For the ECW and WA cyclone centers, the increase is smaller northeast of the center (10% – 20% and 10% – 13% , respectively).

Colle et al. (2013) found that unlike the ECW and WA regions, the number of relatively deep cyclones in the ECL region is increasing during the mid- and late-twenty-first century. A similar result is seen in Fig. 5a. This suggests that the future change in physical processes for the cyclones in the ECL region may be different than the other regions. We calculated the composite precipitation for the S-Center, M-Center, and W-Center cyclones within ECL to explore the precipitation differences. During the historical period, there is a large, well-defined, comma-shaped precipitation region for the S-Center cyclone, with the maximum around 14 mm day^{-1} within the comma head (Fig. 8a). The M-Center cyclone has a smaller precipitation area and a weaker precipitation maximum around 12 mm day^{-1} (Fig. 8c). The precipitation for W-Center cyclone is concentrated just east and northeast of the cyclone center, with a maximum around 11 mm day^{-1} (Fig. 8d). There is slightly more ($\sim 12\%$) moisture content over the warm side of the W-Center cyclone than the M-Center and S-Center cyclones (not shown), since most of these W-Center cyclones are developing farther south in the warmer air. However, the composite upper-level jet ($\sim 51 \text{ m s}^{-1}$ at 250 hPa) for the S-Center cyclone is stronger than the W-Center cyclone ($\sim 42 \text{ m s}^{-1}$ at 250 hPa), with the average storm center located near the left exit region of the jet (not shown). This is associated with 20% – 45% stronger upward motion for S-Center cyclones than M-Center and W-Center cyclones, with a maximum of -0.24 Pa s^{-1} (at 700 hPa), covering a much larger area in the S-Center cyclone. As a result, the S-Center cyclone has more precipitation coverage and a greater maximum than the M-Center and W-Center cyclones (Figs. 8a,c,e). By the late-twenty-first century, the S-Center cyclone has a 25% – 33% increase in the precipitation maximum compared to the historical period (Fig. 8a), with a maximum rate increase of 3.3 mm day^{-1} (Fig. 8b). The precipitation increase of M-Center cyclones (Fig. 8d) has a similar pattern to the S-Center cyclone, but the increase is smaller (20% – 30%). Meanwhile, the increase for W-Center cyclone is the smallest increase, around 15% (Fig. 8f).

A time series of the mean precipitation and the maximum precipitation rate were calculated around each cyclone center (black box in Fig. 1), which covers most the precipitation area. There is a significant increasing trend for both the mean and maximum

precipitation for the ECL centers during twenty-first century (Fig. 9). The maximum precipitation around the cyclone centers within ECL increases by approximately 26% (Fig. 9a), from about 27 mm day^{-1} in the historical period to about 34 mm day^{-1} at the end of twenty-first century. The maximum precipitation increase for WA is about 15% (Fig. 9b), while the increase for ECW is about 21% (not shown). The increase trend of the ECL and WA maximum precipitation in Figs. 9a and 9b, respectively, is significant at 95% level using the Student's *t* test. The model spread in maximum precipitation within all regions is very large. For example, the higher-resolution HadGEM2-CC has significantly greater (40% – 50%) maximum precipitation than the three low-resolution (between 2° and 2.5°) models (GFDL-ESM2M, IPSL-CM5A-LR, and MIROC-ESM-CHEM) within the WA region. The mean precipitation around the cyclone center (Figs. 9c,d) has a similar result within the ECL, increasing from about 7.7 mm day^{-1} during historical period to about 9.6 mm day^{-1} by the end of twenty-first century (about 25%), while the increase of WA is smaller (about 13%). The increase trend of the ECL mean precipitation in Fig. 9c is significant at the 95% level, and the WA mean precipitation in Fig. 9d is significant at 90% level using the Student's *t* test. The model spread for mean precipitation is much smaller than the maximum precipitation.

The future change in the distribution of the mean and maximum precipitation for the same black box around the cyclone was examined. For cyclone centers within ECL during the historical period (Fig. 10a), the peak in maximum precipitation averaged for all models ranges from 12 to 28 mm day^{-1} but has a long tail toward heavier amounts. Through the twenty-first century, there is a shift toward greater precipitation amounts ($>36 \text{ mm day}^{-1}$; Fig. 10c). The heaviest precipitation ($>56 \text{ mm day}^{-1}$) has a large increase, about 150% (Fig. 10e) for the cyclone centers within ECL. The WA, which has a narrower precipitation distribution, also has a trend toward heavier precipitation, but the increase of $>56 \text{ mm day}^{-1}$ is only about half as large as ECL (Fig. 10f). The future changes in the distribution of mean precipitation around the cyclone centers are similar to the results of maximum precipitation, having a shift toward the heavy precipitation, but the variation among models is relatively small.

Figure 11 shows the number of cyclone events over the ECL region for the extreme daily precipitation rates averaged within the black box in Fig. 1 around the cyclone. These extreme precipitation cyclone events are defined using the 95th percentile of the mean precipitation rate within the black box in Fig. 1. The extreme precipitation rate thresholds are 18.4 mm day^{-1} for

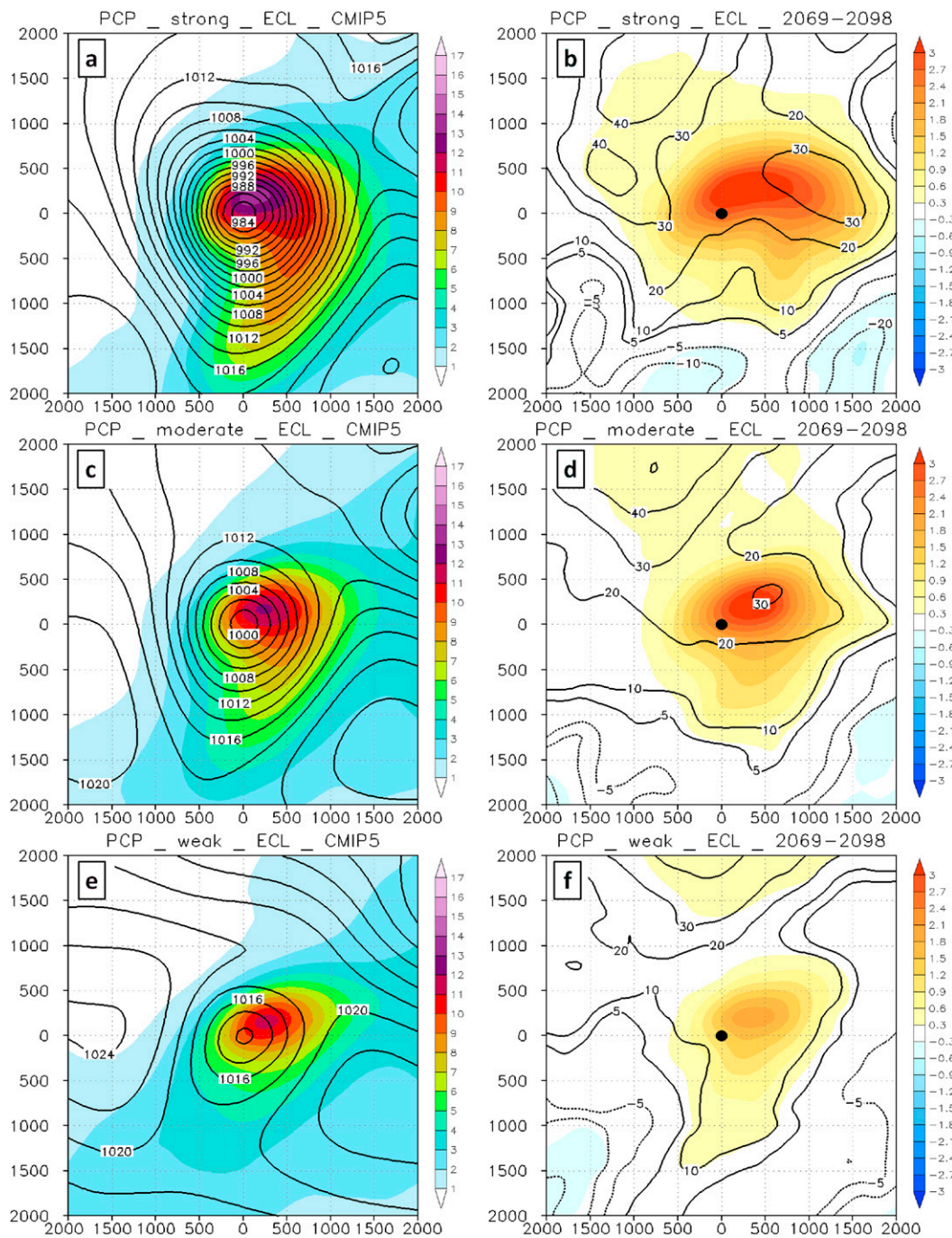


FIG. 8. As in Fig. 7, but for the (a),(b) S-, (c),(d) M-, and (e),(f) W-Center cyclones within ECL.

1979–2004, 19.2 mm day^{-1} for 2009–38, 20.6 mm day^{-1} for 2039–68, and 22.5 mm day^{-1} for 2069–98 cool seasons. For the historical period, over 90% of the extreme cases are concentrated at $18\text{--}26 \text{ mm day}^{-1}$, while during the late-twenty-first century, the extreme rates shift to $22\text{--}32 \text{ mm day}^{-1}$. Meanwhile, in the late-twenty-first century, it has a longer tail toward to the most extreme values.

d. Physical processes responsible for future precipitation changes

The comparisons in section 3c confirm that the ECL cyclone centers have a larger precipitation increase than the ECW and WA, and the S-Center cyclone has a larger increase than the relatively weaker centers within the

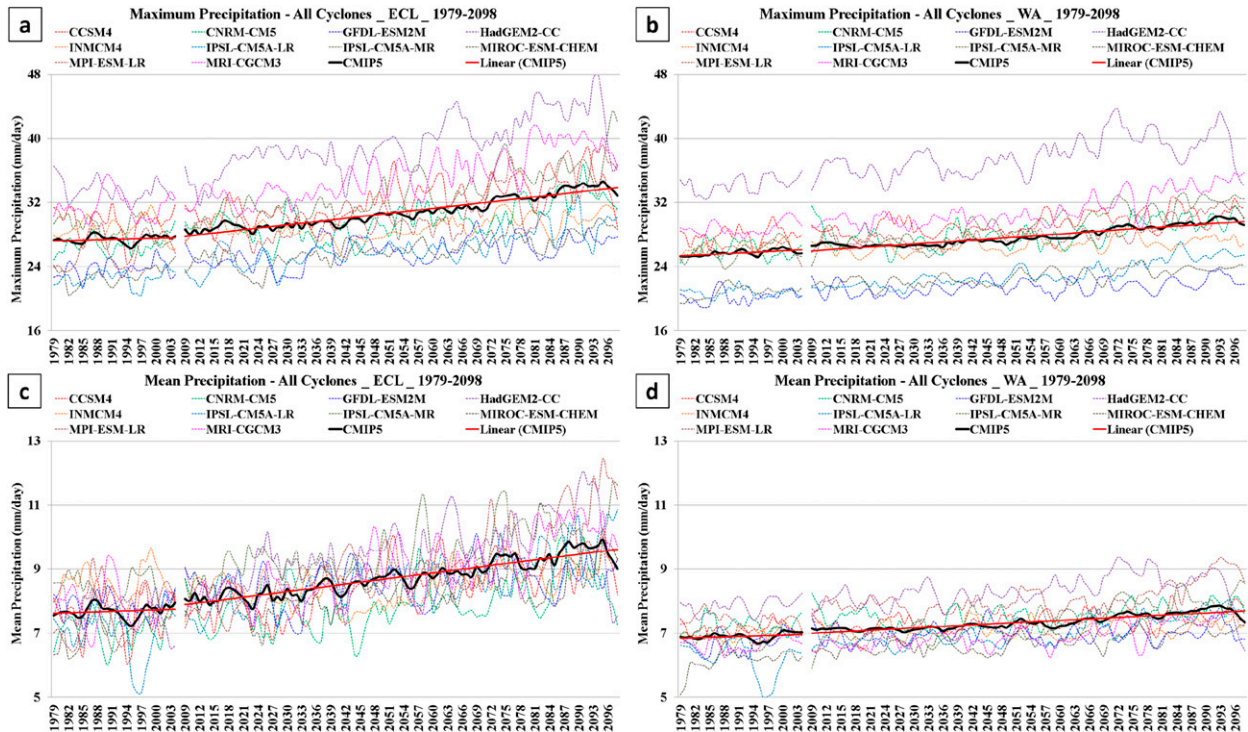


FIG. 9. The time series (3-yr running mean) of maximum precipitation around the cyclone center from 1979 to 2098 cool seasons for the cyclone centers within (a) ECL and (b) WA. The black line is the CMIP5 ensemble mean, the red line is the linear trend of the CMIP5 mean, and the dashed lines are for the individual models. (c),(d) As in (a),(b), but for the mean precipitation within the small black box in Fig. 1.

ECL region. In this section, we investigate the physical processes responsible for those differences.

In the CMIP5 RCP8.5 experiment, the surface temperature increase over land is greater than over the ocean toward the end of the twenty-first century. The Arctic region is projected to warm the most, while the temperature increase has a minimum in the North Atlantic and Southern Oceans (IPCC AR5, chapter 12). As a result, for the cyclones over eastern North America and the western Atlantic, the 850-hPa temperature increase is larger over the northwest side of the cyclone center (over or close to the North American continent) and smaller over the southeast side (over or close to the North Atlantic ocean; Fig. 12). The increase of 850-hPa temperature over the precipitation maximum region (hereafter P-MAX, immediately northeast of the cyclone center) of ECL cyclone centers is 4–4.5 K. Meanwhile, the increases for the ECW (3–3.5 K) and WA (about 3 K) cyclone centers are smaller (Figs. 12a–c). Near the cyclone center, the 850-hPa temperature increases over the P-MAX of S-Center and M-Center cyclones are very close, 4–5 K, but the increase of W-Center cyclone is around 3.5 K (Figs. 12d–f). The changes in integrated moisture content at 850–250 hPa

(not including the lower-level moisture because data are not available) and the temperature at that level are consistent with the Clausius–Clapeyron relation, approximately a 6.5% increase in moisture content per kelvin increase in temperature. Similar to the 850-hPa temperature increases, over the P-MAX the moisture increase for the ECL cyclone centers (around 30%) is larger than the ECW (around 25%) and WA (around 22%) centers (Figs. 13a–c). Within ECL, the moisture increases over the P-MAX for S-Center (around 35%) and M-Center (around 34%) cyclones are larger than the increase of W-Center cyclones (around 26%; Figs. 13d–f). These results are qualitative, consistent with the future increases of precipitation. The precipitation increase for the ECL cyclone centers is larger than ECW and WA (Fig. 7), and the increase of S-Center precipitation is larger than the M-Center and W-Center cyclones within ECL (Fig. 8). Thus, the differences in the lower-tropospheric temperature (and moisture) increase are important to the future precipitation change for the cyclone centers in different regions.

However, the precipitation response ($\% K^{-1}$) to the temperature increase also varies for cyclone centers in

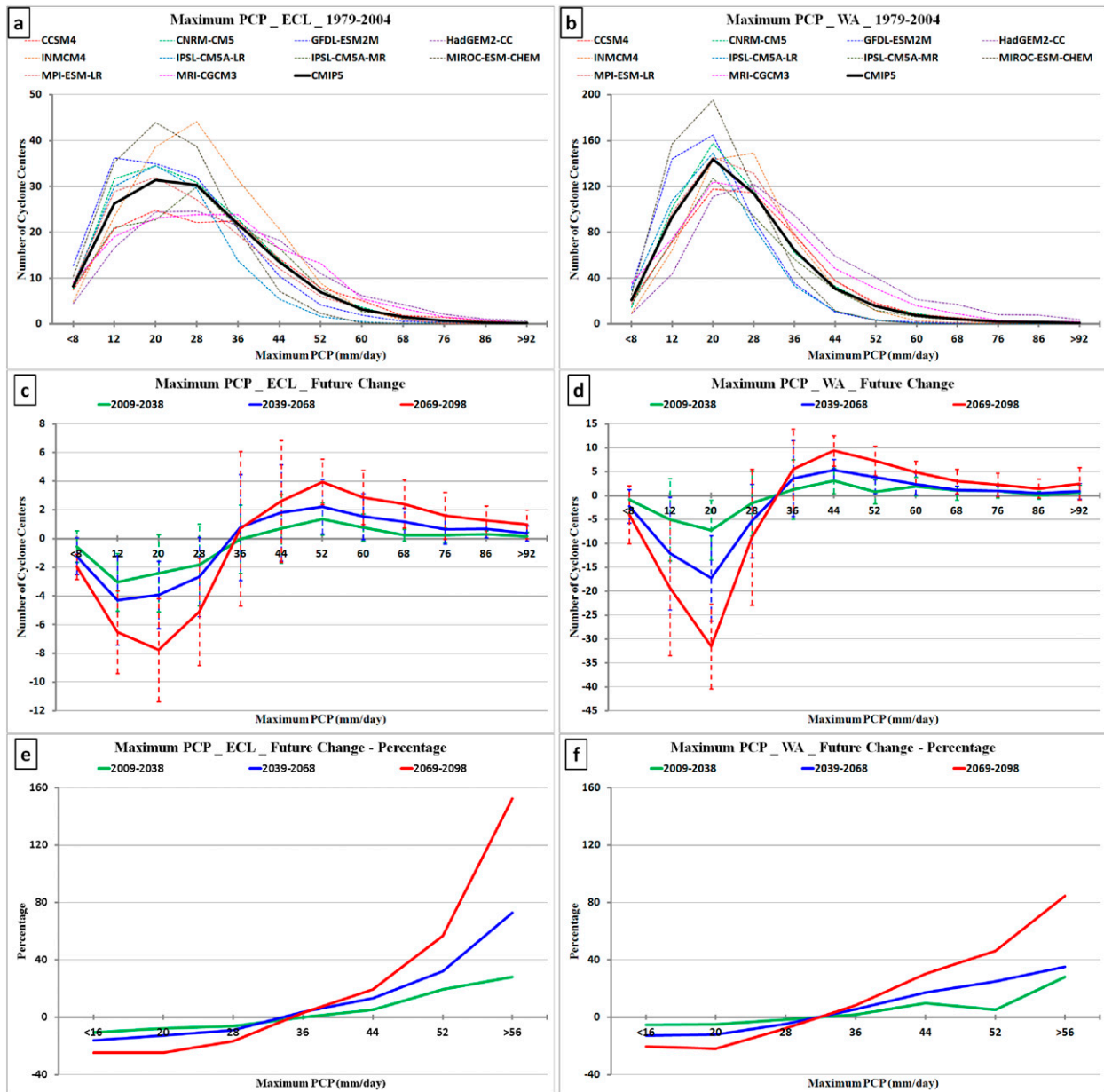


FIG. 10. The distribution of maximum precipitation rate around cyclone center: (a),(b) historical mean, (c),(d) future changes, and (e),(f) percentage changes. (left) Results for cyclone centers within ECL and (right) results for centers within WA.

different regions. For example, over the P-MAX it is approximately $6.0\% \text{ K}^{-1}$ for the ECL, approximately $5.1\% \text{ K}^{-1}$ for the ECW, and approximately $3.9\% \text{ K}^{-1}$ for the WA centers, indicating that there must be some other factors impacting the precipitation change. We explored the related dynamic and thermodynamic daily averaged fields, including low-level wind speed, upper-level jet, vertical motion, static stability, and warm advection, which may be related to the different precipitation responses for different cyclones.

The field with the largest difference in the future changes for the ECL, ECW, and WA cyclone centers is the moist static stability [calculated following Durran and Klemp (1982) and Jiang and Doyle (2009)]. Under climate change over the Northern Hemisphere cool season the upper troposphere warms more than the lower troposphere at mid-to-low latitudes ($<55^\circ\text{N}$). Meanwhile, at higher latitudes ($>55^\circ\text{N}$), because of the amplification near the surface over continental regions at high latitudes, the low-level temperature increase is

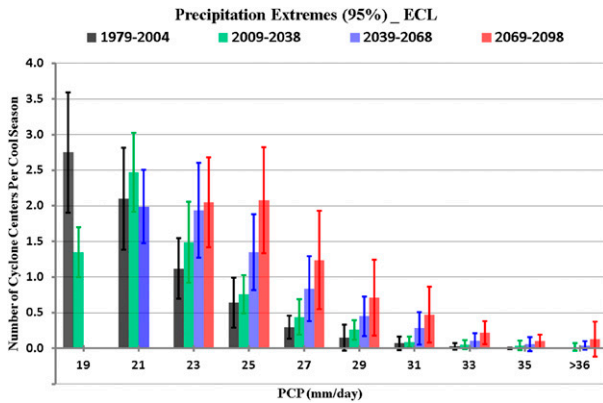


FIG. 11. The distribution of precipitation extremes (95th percentile) around the cyclone centers (within the small black box in Fig. 1) within ECL region, for the historical and three future periods. The error bars are plus or minus one standard deviation.

larger than at upper levels at high latitude (IPCC AR5, chapter 12). As a result, the atmosphere becomes less stable at the high latitudes, especially over the land, while it becomes more stable over midlatitudes,

especially over the Atlantic Ocean where the surface temperature increase is much smaller (Frierson 2006). The moist static stability changes at 850–500 hPa (Fig. 14) around the ECL, ECW, and WA cyclone centers over eastern North America and the western Atlantic are consistent with that. Overall, it becomes less stable in the northern and western side of the cyclone center and more stable in the south and east side. The boundary between the negative and positive change is close to or just over the cyclone center during the late-twenty-first century (Fig. 14). Around the ECL cyclone center and over the P-MAX, the stability decreases by 5%–10%, which is more favorable for the precipitation increase. There is very little change for the ECW centers. However, the stability increases by 5%–10% for the WA centers, which is one of the reasons responsible for the weaker precipitation response in this region. We also look at future changes in several other factors related to the ECL, ECW, and WA cyclone centers. For example, the upper-level jet becomes slightly stronger (~5%) for all the ECL, ECW, and WA cyclone centers and has similar positions (centers are located at the left

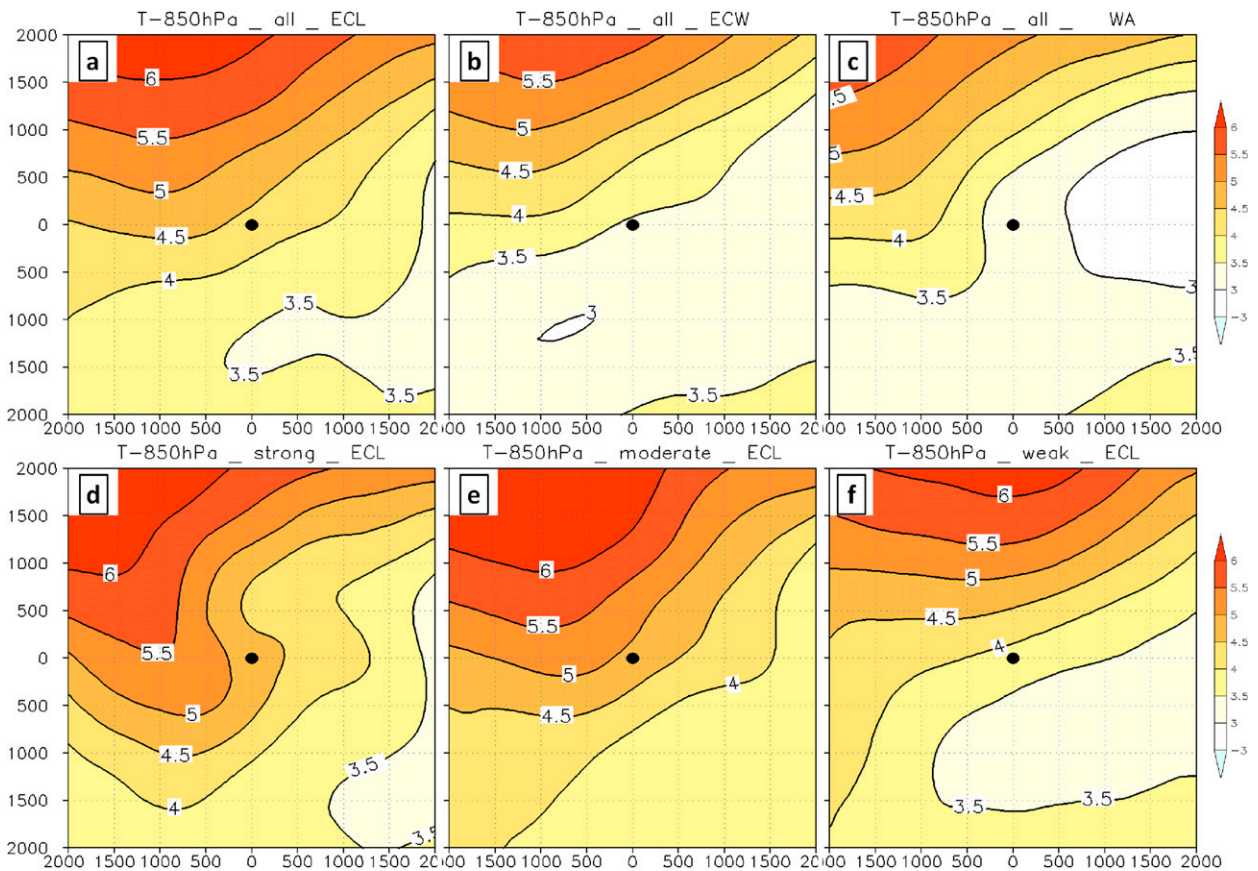


FIG. 12. The future changes of 850-hPa temperature (colors; K) around the cyclone (axes in km) for 2069–98 cool seasons for CMIP5 mean for the cyclone centers within (a) ECL, (b) ECW, and (c) WA and for the (d) S-, (e) M-, and (f) W-Center cyclones within ECL.

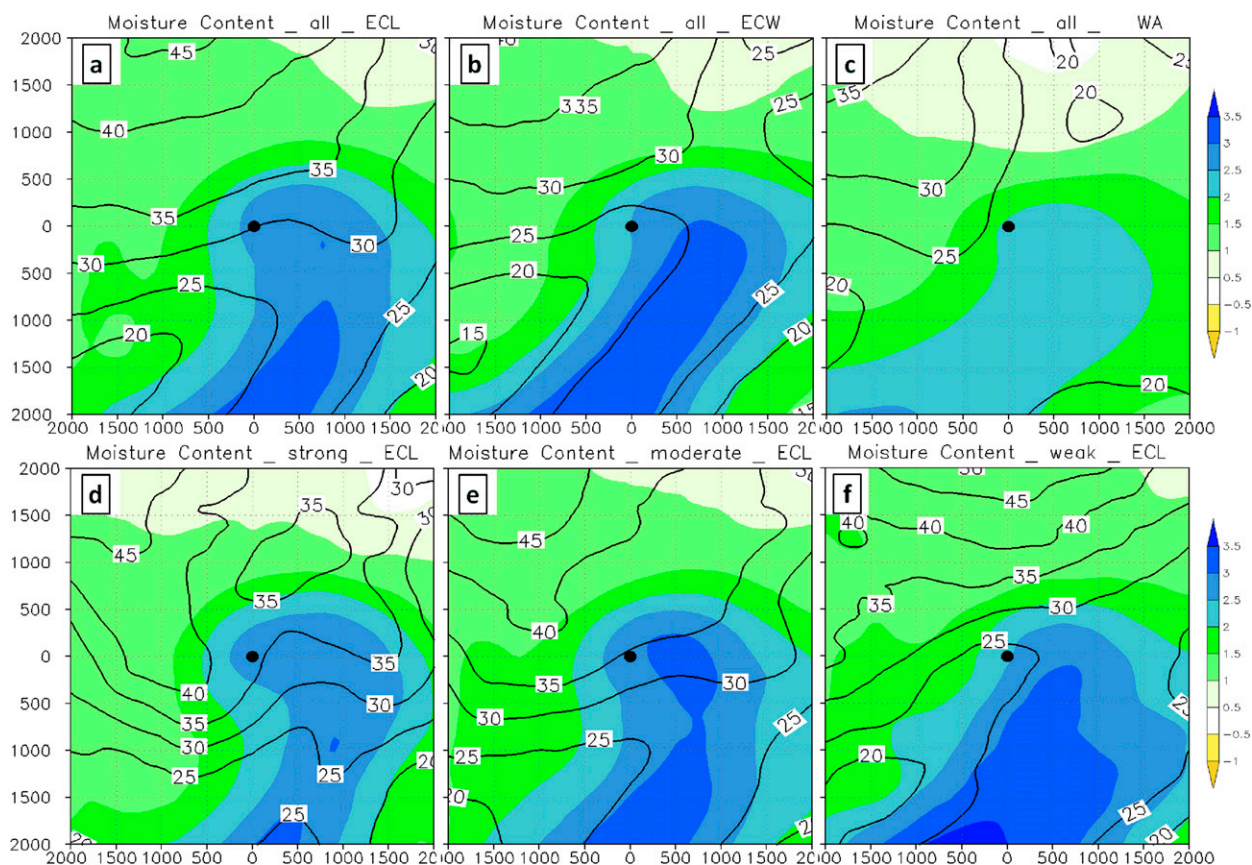


FIG. 13. The future changes of 850–250-hPa moisture content (colors; kg m^{-2}) and the percentage changes (contours; %) around the cyclone (axes in km) for 2069–98 cool seasons for CMIP5 mean for the cyclone centers within (a) ECL, (b) ECW, and (c) WA and for the (d) S-, (e) M-, and W-Center cyclones within ECL.

side of the jet exit). The upward motion becomes slightly stronger ($\sim 5\%$) over the PMAX by the late-twenty-first century for the mean of ECL centers, while there is very little change for the WA centers.

The precipitation-related fields are also compared for the S-Center, M-Center, and W-Center cyclones within ECL. The stability around the S-Center and M-Center cyclones has a 5%–13% decrease, while W-Center cyclone is close to the boundary between the negative and positive changes (Figs. 14d–f). For the low-level wind speed (850 hPa), there is a small increase ($\sim 5\%$) over the warm side of S-Center cyclone, which is favorable to the moisture transport, while there is no change for the M-Center cyclones and a slight decrease ($\sim 5\%$) for the W-Center cyclones. For the vertical motion, there is an approximate 17% increase in upward motion east of the S-Center cyclone and an approximate 10% increase for the M-Center cyclones, but this increase in upward motion disappears for the W-Center cyclone. The upper-level jet (250 hPa) becomes slightly stronger ($\sim 5\%$) for all of the S-Center, M-Center, and W-Center

cyclones. However, the S-Center cyclones are located just at the left side of the jet exit region, which is favorable to the upward motion, while the W-Center cyclones are located close to the jet center (not shown).

e. A closer look at future precipitation extremes in the ECL region

In addition to the mean precipitation changes in previous sections, the future changes of extreme precipitation and its relation to cyclone deepening are examined in this section. Colle et al. (2013) found that there is an increase in the number of intense cyclones within ECL. To explore the potential relationship between the heavier precipitation and the deeper cyclones within ECL, we examined those cyclone cases associated with the precipitation extreme cases within ECL in Fig. 11. During the historical period, most of these cyclone cases deepen quickly, with about 70% of these centers deepening over 2 hPa in 6 h (Fig. 15a). During the mid- and late-twenty-first century there is a significant shift toward a more rapid deepening rate, ranging

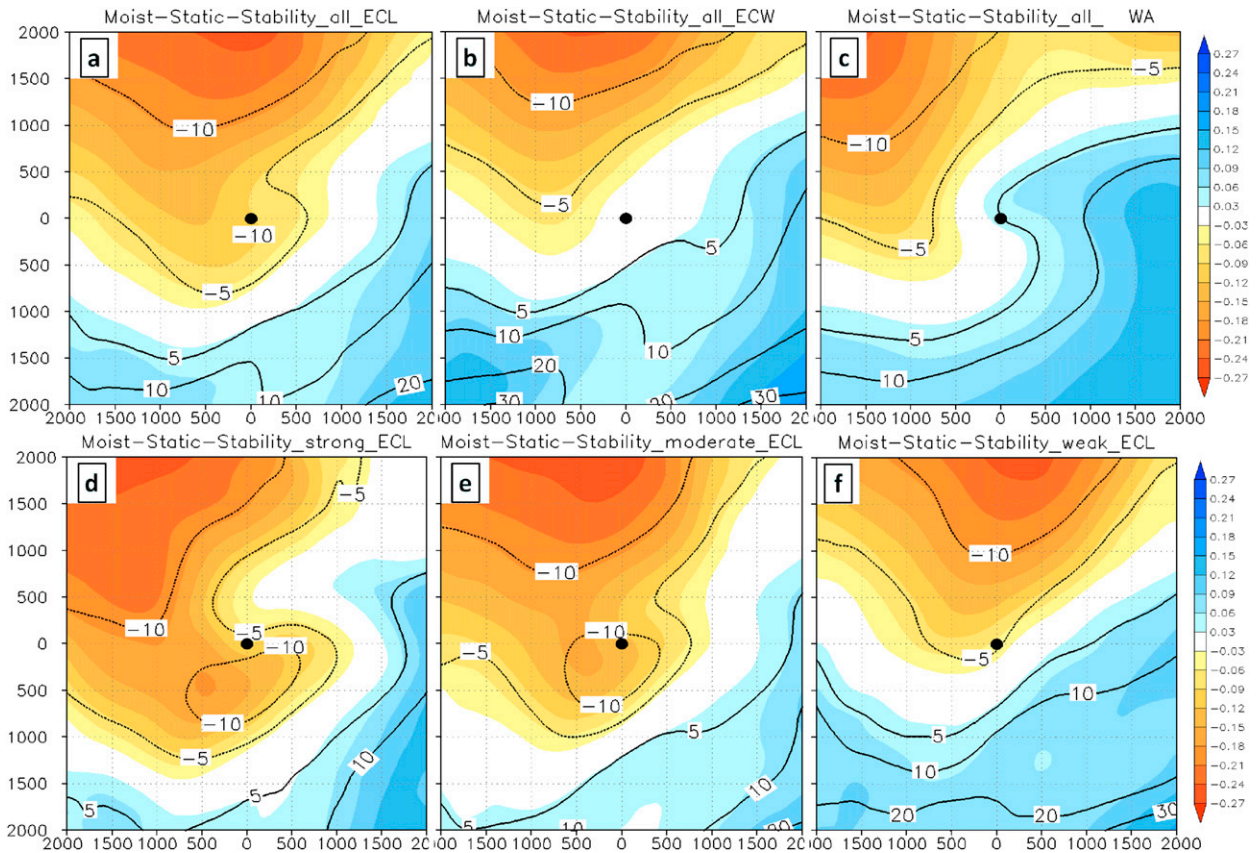


FIG. 14. As in Fig. 13, but for 850–500-hPa moist static stability ($S^{-2} \times 10^{-4}$).

from around $-2 \text{ hPa} (6 \text{ h})^{-1}$ during the historical period to -8 and $-10 \text{ hPa} (6 \text{ h})^{-1}$ during the mid- and late-twenty-first century, respectively (Fig. 15b).

The evolution of those cyclone cases associated with extreme precipitation (95% percentile) within the ECL region was examined backward in time 60 h from the time the cyclone was the deepest (hour 0). Figure 16 shows the ensemble-mean evolution of central pressure, low-level temperature, precipitation, and 850–500-hPa latent heating rate for these extreme cases. We calculated the 850–500-hPa latent heating rate following the approach used by Emanuel et al. (1987). At 60 h before the deepest time, the cyclone central SLP during the future periods is very close to or slightly larger (2069–98) than the SLP in the historical period (Figs. 16c,d); however, the increases of precipitation and LHR already exist. During the 2039–68 and 2069–98 periods, the center deepens more quickly for most of the 60-h development, especially for the mid- and late-twenty-first century (Figs. 16c,d). Meanwhile, there is a 5%–20% decrease in the surface temperature gradient (Figs. 16a,b), a 10%–30% increase in precipitation (Figs. 16e,f), and a 10%–25% increase in the latent

heating rate (Figs. 16g,h). Although the low-level baroclinicity is decreasing, those cyclone cases associated with the extreme precipitation within the ECL region are becoming deeper. Therefore, it is hypothesized that the latent heat release from precipitation compensates the loss in baroclinicity, thus resulting in cyclone deepening.

To further examine this hypothesis, the SLP, precipitation, meridional moisture flux (850–250 hPa), warm advection (850 hPa), surface temperature gradient, Eady growth rate (850–500 hPa), and upper-level jet (250 hPa) around the cyclone center were calculated for each time step. The fields at -12 h (12 h before the deepest center within the ECL) are discussed, which is when the precipitation is the heaviest (Fig. 16e).

Figure 17 shows the historical-mean fields at -12 h when the cyclone is relatively deep (993 hPa), with the maximum precipitation ($>24 \text{ mm day}^{-1}$) northeast of the cyclone center (Fig. 17a). There is strong moisture flux (850–250 hPa) over the warm sector part of the cyclone (Fig. 17b) and prominent warm advection (850 hPa) to the northeast of the cyclone center (Fig. 17c). In addition, the cyclone center is located in a

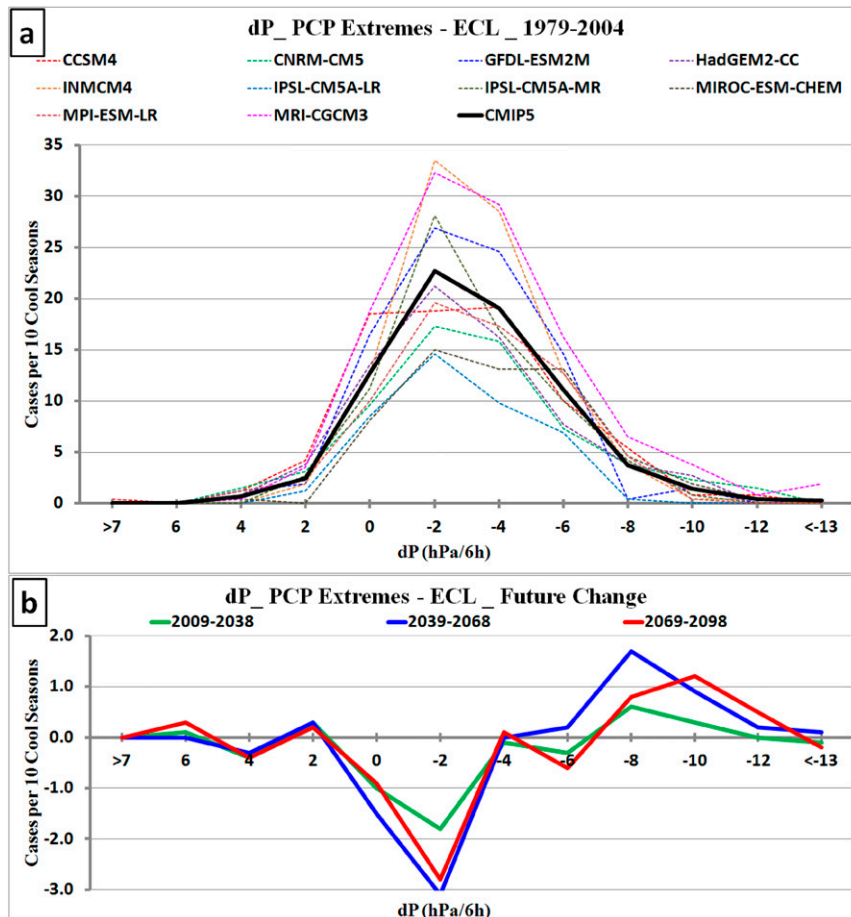


FIG. 15. The distribution of cyclone deepening rate for the ECL cyclone centers associated with the extreme precipitation for the (a) historical mean and (b) future changes.

region of strong, upper-level divergence near the left side of a cyclonic jet exit region and the right entrance of an anticyclonic jet (Fig. 17d). Meanwhile, the surface temperature gradient and Eady growth rate (850–500 hPa) are strong over the northeast side of the center (Figs. 17e,f). All of these conditions are conducive to the heavy precipitation and the cyclone developing.

During late-twenty-first century at -12 h, the baroclinicity decreases around the cyclone center (Figs. 18e,f), with the surface temperature gradient decreasing by 10%–20% and the 850–500-hPa Eady growth rate decreasing by about 5%. There is no significant change for the warm advection around the cyclone center (Fig. 18c). Meanwhile, there is a large increase (around 30%) in the moisture flux over the warm side of the cyclone (Fig. 18b), which is mainly due to the local moisture increase and enhanced by a slightly stronger low-level wind speed. There is also a small increase in upper-level jet ($\sim 10\%$) over the south side of the jet, somewhat far away from the cyclone center (Fig. 18d).

As a result of these changes, the mean cyclone central SLP is about 2 hPa deeper at the deepest point within the ECL for the late-twenty-first century, while the precipitation increases by 20%–30% over the warm side of cyclone center (Fig. 18a). Given that the baroclinicity is decreasing and other fields do not exhibit significant changes, this provides more evidence that deeper future cyclones are the result of an increase in latent heat release from precipitation.

4. Conclusions and discussion

This study explored the future change in precipitation associated with extratropical cyclones during the cool season over eastern North America and the western Atlantic using the historical and future (RCP8.5) experiments from 10 CMIP5 models. We also compared the future precipitation changes around cyclone centers within the ECL, ECW, and WA regions in Fig. 2 as well as the S-Center (<990 hPa), M-Center (990–1005 hPa),

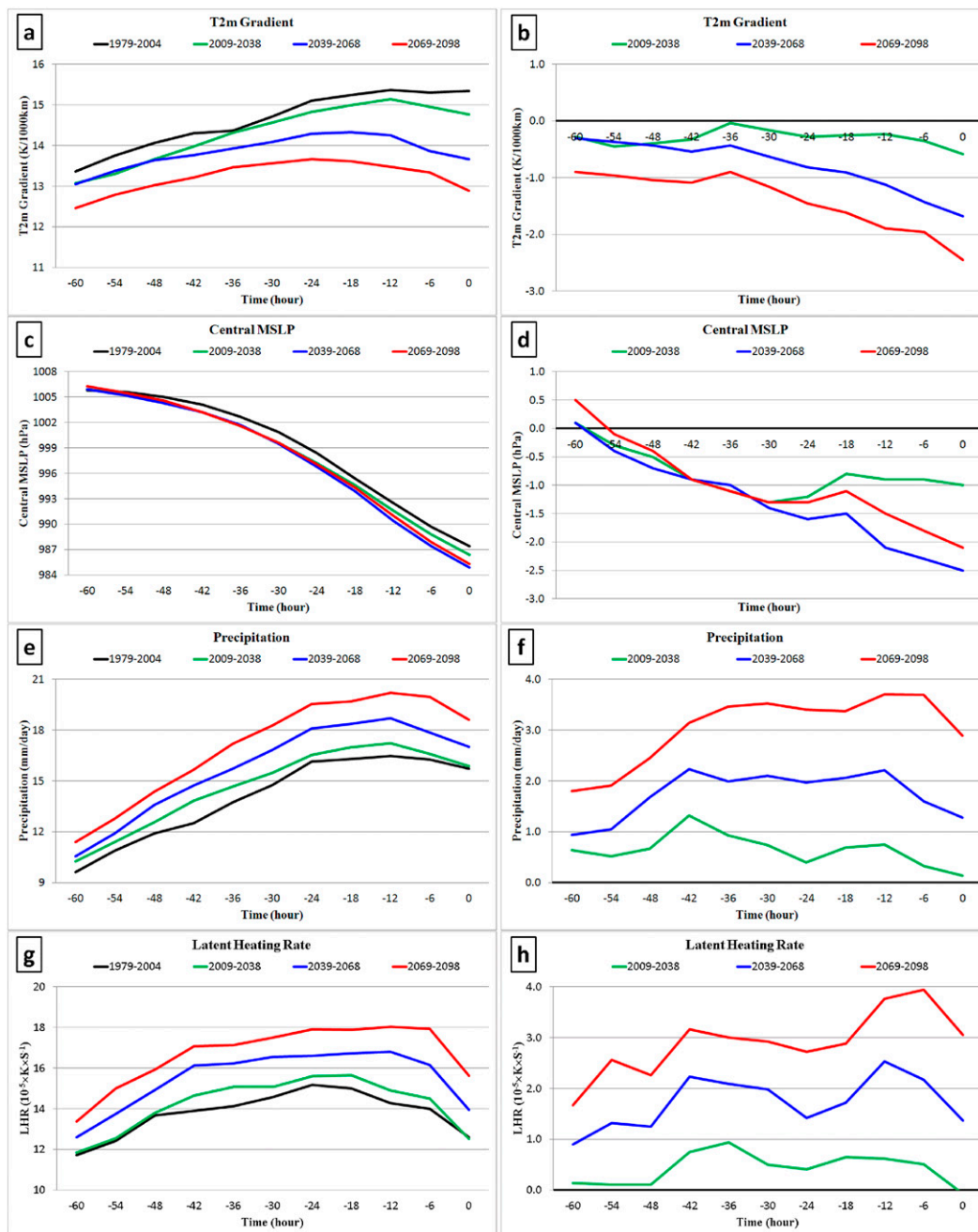


FIG. 16. The evolution of the cyclones associated with the precipitation extreme cases within ECL. The x axis is the time (h) before the deepest center within ECL for the (a),(b) surface temperature gradient; (c),(d) central SLP; (e),(f) precipitation; and (g),(h) 850–500-hPa latent heating rate (10^{-5} K s^{-1}) around the cyclone center. (left) The mean results for the historical and future periods and (right) the future changes.

and W-Center (>1005 hPa) cyclones within the ECL, using cyclone-relative composites where possible. Last, we examined the evolution of cyclone deepening within the ECL for the precipitation extreme (>95 th percentile) events for the historical and future periods. The major findings of this study are as follows:

- 1) The CMIP5 models with better performance in simulating extratropical cyclones tend to have smaller mean absolute error in mean precipitation during the cool season over eastern North America and the western North Atlantic, although there are some exceptions. Overall, the ensemble mean of the 10

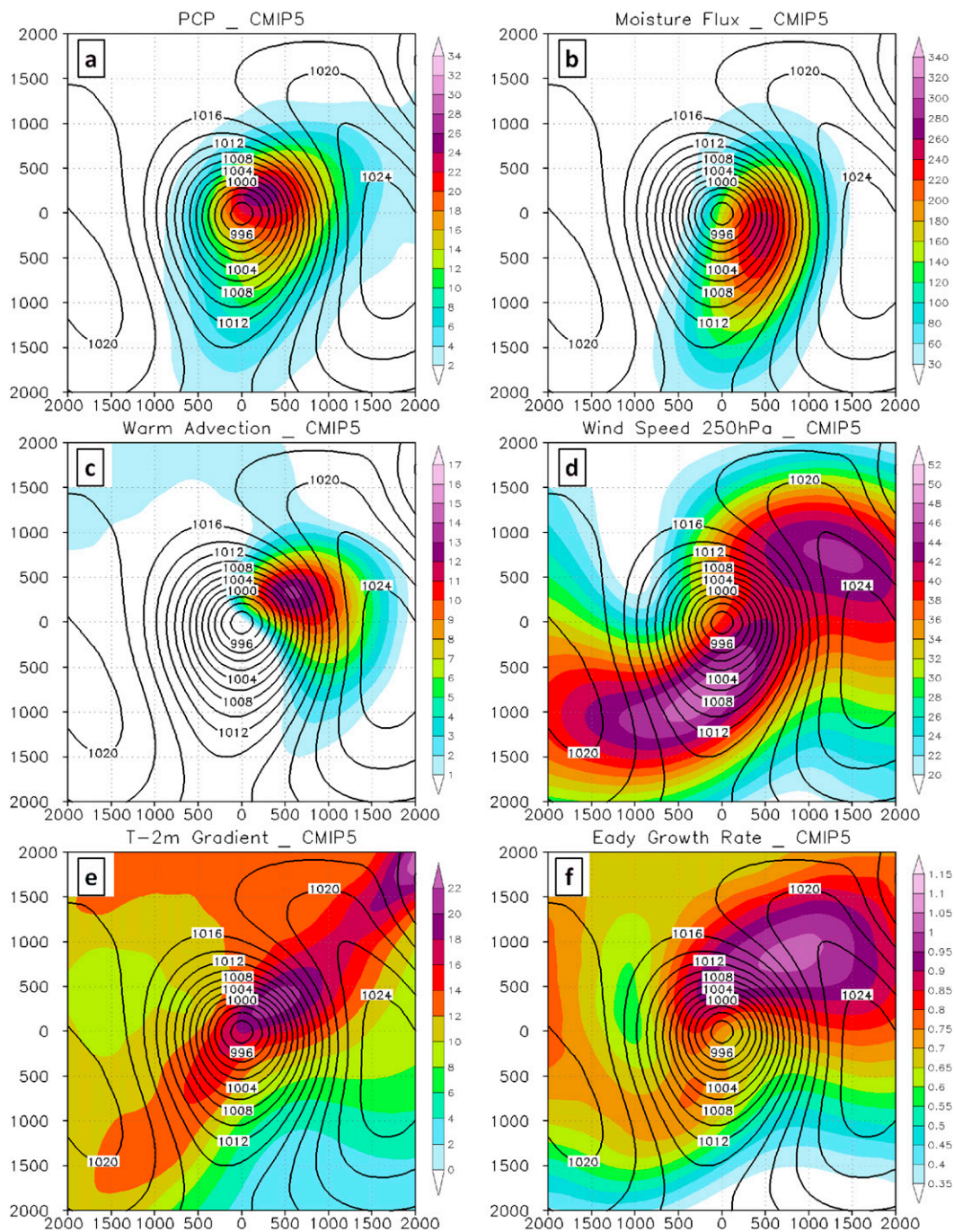


FIG. 17. The composite fields around the cyclone centers (axes in km) associated with ECL precipitation extreme cases at hour -12 in Fig. 16 for the historical period. The contours are SLP (hPa), and the colors are (a) precipitation rate (mm day^{-1}), (b) 850–250-hPa moisture flux ($\text{kg m}^{-1} \text{s}^{-1}$), (c) 850-hPa warm advection (K s^{-1}), (d) 250-hPa wind speed (m s^{-1}), (e) surface temperature gradient [K (1000 km)^{-1}], and (f) 850–500-hPa Eady growth rate (day^{-1}).

CMIP5 models has a smaller mean absolute error than individual models.

- 2) The cyclone-relative precipitation contributes from 60% at relatively lower latitudes ($\sim 25^\circ\text{N}$) to over

90% at relatively higher latitudes ($>40^\circ\text{N}$) to the total precipitation amount during the cool season over eastern North America and the western Atlantic. During the late-twenty-first century, most of the precipitation

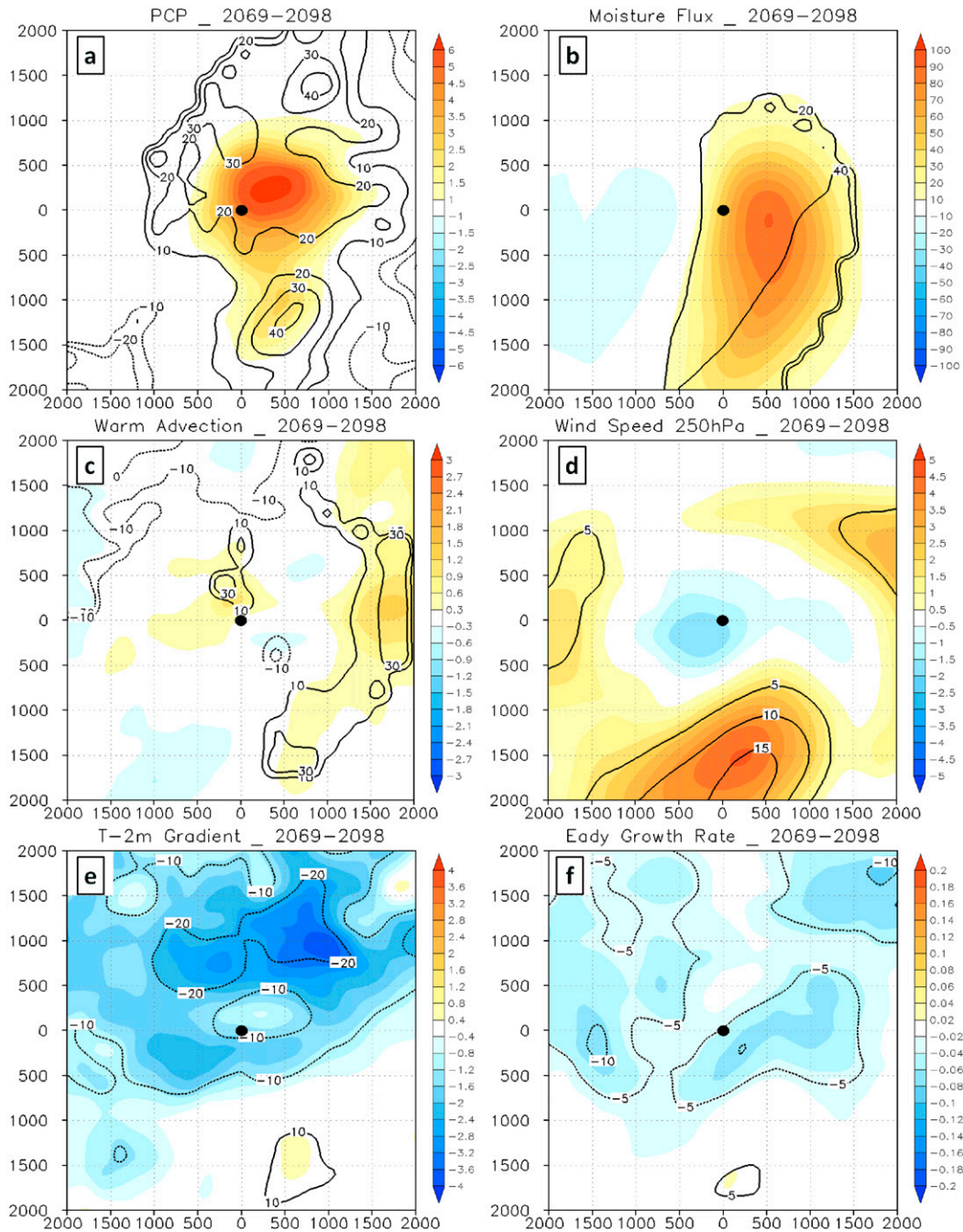


FIG. 18. As in Fig. 17, but for the future changes in late-twenty-first century (2069–98). The contours are the percentage of the changes.

amount increase (Figs. 5e–h) comes from the S-Center and M-Center cyclones because of the large precipitation rate increase (Figs. 5i–l) associated with each cyclone center and a slight increase in the cyclone center density (Fig. 5a–d) over the land, while the increase of the W-Center precipitation rate is cancelled by the decrease of weak cyclone frequency.

3) Comparing cyclone centers within different regions, the ECL cyclone centers exhibit the largest increase in both absolute value and percentage increases for cyclone-relative precipitation rate over the P-MAX, while the WA centers have the smallest increase (10%–13%) during the late-twenty-first century. The ECL centers have the largest low-level temperature

(and moisture) increase, a 5%–10% decrease in static stability around the center, and a small increase (~5%) in upward motion. Meanwhile, the WA centers have the smallest low-level temperature (and moisture) increase and an increase (5%–10%) in static stability over the warm side of the cyclone. The differences of other factors, such as the upper-level jet, are relatively small.

- 4) For the cyclone centers within the ECL region, the S-Center cyclones have a large increase (about 30%) in precipitation rate over the P-MAX, but the increase for the W-Center cyclone is much smaller (about 15%). The increase of low-level temperature (and therefore moisture) is slightly larger for the S-Center than the W-Center cyclone over the P-MAX, since the S-Center cyclone tends to be farther north where the low-level temperature increase is larger. Static stability decreases around the S-Center cyclone (5%–13%), but there is no change for the W-Center cyclone. Meanwhile, there is an (~17%) increase in the upward motion and a small increase (~5%) in the 850-hPa wind speed over the warm side of the S-Center cyclone, which is favorable to the poleward moisture transport (not shown). For the W-Center cyclone, there is no change for the upward motion and a small decrease (~5%) for the 850-hPa wind speed.
- 5) There is a significant shift toward heavier precipitation in the distribution of the cyclone-relative precipitation during the twenty-first century, especially for the ECL region. The cyclone cases associated with extreme precipitation within ECL exhibit a 20%–30% increase in the precipitation rate and a 10%–25% increase in the latent heating rate over the warm frontal region. The increases of precipitation and latent heating rate precede the increase of cyclone rapid deepening in the future periods. Given a 10%–20% decrease in surface temperature gradient and an approximate 5% decrease in 850–500-hPa Eady growth rate, the stronger latent heat release over the warm side of the cyclone from heavier precipitation plays an important role in cyclone rapid deepening for the extreme cyclone cases.

This study focused on the precipitation associated with extratropical cyclones during cool season and compared the changes for cyclones in three different regions (ECL, ECW, and WA) over eastern North America and the western Atlantic. Although the temperature increases across all of the three regions, there are large regional differences in lower-tropospheric temperature and moisture changes, which cause large

variance in the precipitation changes associated with the cyclone centers in those regions. The future precipitation change also varies for the cyclones in different intensity within the same ECL region. During the twenty-first century, the S-Center cyclone located over the relatively higher latitudes has large, low-level temperature (and moisture) increase and a decrease in static stability. As a result, the S-Center cyclone has a larger precipitation increase than the M-Center and W-Center cyclones and enhances the feedback between the precipitation increase and cyclone deepening.

Although studies suggest a decrease in extratropical cyclones over eastern North America and the western Atlantic because of the baroclinicity decrease under global warming (Chang 2013; Zappa et al. 2013); the results in this study indicate that over the ECL region, the latent heat will become more important to the rapid deepening of cyclones in the future. Over the ECL region, the precipitation increase is larger than the ECW and WA region mainly because of the larger low-level temperature (and moisture) increase and the decrease in static stability. Given these favorable environmental conditions within this ECL region, some intense cyclones accompanied with heavy precipitation will enhance the strong positive feedback between the latent heat release from precipitation and the cyclone deepening, bringing more rapid deepening rate and extreme intense cyclone cases. This is consistent with the feedback mechanism demonstrated by some previous studies (Lackmann and Gyakum, 1999; Lackmann 2002). In the cyclone cases associated with the extreme precipitation within the ECL region, the future increases in precipitation and latent heating rate precede the more rapid cyclone deepening in the mid- and late-twenty-first century. Given the decrease of low-level baroclinicity, the stronger latent heat release will play an important role in the cyclone rapid deepening in the future period. Marciano et al. (2015) also conclude that the enhanced latent heat release is responsible for this regional increase in future cyclone intensity based on their WRF simulations of 10 “Miller-A” cyclones. More studies are needed to improve our understanding of the detailed impacts of enhanced latent heat release on a broad distribution of extratropical cyclones under climate change. Willison et al. (2013) demonstrate that the feedback between latent heat release and cyclone deepening in the model is highly sensitive to the horizontal resolution. Because of the limitations of resolving mesoscale latent heat processes in current, coarse-resolution global climate models, it is necessary to involve more experiments using high-resolution models, which can simulate the diabatic processes in cyclones more realistically.

Acknowledgments. We thank the three reviewers for their valuable comments, which helped to improve our manuscript. We acknowledge the World Climate Research Programme Working Group on Coupled Modelling, which is responsible for CMIP, and we thank the climate modeling groups (listed in Table 1 of this paper) for producing and making available their model output. The authors acknowledge the support of NOAA Climate Program Office Modeling, Analysis, Predictions, and Projections (MAPP) Program as part of the CMIP5 Task Force under Grant NA11OAR4310104.

REFERENCES

- Adler, R. F., and Coauthors, 2003: The Version-2 Global Precipitation Climatology Project (GPCP) Monthly Precipitation Analysis (1979–present). *J. Hydrometeor.*, **4**, 1147–1167, doi:10.1175/1525-7541(2003)004<1147:TVGPCP>2.0.CO;2.
- Agel, L., M. Barlow, J. H. Qian, F. Colby, E. Douglas, and T. Eichler, 2015: Climatology of daily precipitation and extreme precipitation events in the northeast United States. *J. Hydrometeor.*, **16**, 2537–2557, doi:10.1175/JHM-D-14-0147.1.
- Allan, R. P., and B. J. Soden, 2008: Atmospheric warming and the amplification of precipitation extremes. *Science*, **321**, 1481–1484, doi:10.1126/science.1160787.
- Allen, M. R., and W. J. Ingram, 2002: Constraints on future changes in climate and the hydrologic cycle. *Nature*, **419**, 224–232, doi:10.1038/nature01092.
- Bengtsson, L., K. I. Hodges, and N. Keenlyside, 2009: Will extratropical storms intensify in a warmer climate? *J. Climate*, **22**, 2276–2301, doi:10.1175/2008JCLI2678.1.
- Catto, J. L., L. C. Shaffrey, and K. I. Hodges, 2010: Can climate models capture the structure of extratropical cyclones? *J. Climate*, **23**, 1621–1635, doi:10.1175/2009JCLI3318.1.
- , C. Jakob, and N. Nicholls, 2015: Can the CMIP5 models represent winter frontal precipitation? *Geophys. Res. Lett.*, **42**, 8596–8604, doi:10.1002/2015GL066015.
- Chadwick, R., I. Boutle, and G. Martin, 2013: Spatial patterns of precipitation change in CMIP5: Why the rich do not get richer in the tropics. *J. Climate*, **26**, 3803–3822, doi:10.1175/JCLI-D-12-00543.1.
- Chang, E. K., 2013: CMIP5 projection of significant reduction in extratropical cyclone activity over North America. *J. Climate*, **26**, 9903–9922, doi:10.1175/JCLI-D-13-00209.1.
- , and S. Song, 2006: The seasonal cycles in the distribution of precipitation around cyclones in the western North Pacific and Atlantic. *J. Atmos. Sci.*, **63**, 815–839, doi:10.1175/JAS3661.1.
- Colle, B. A., 2003: Numerical simulations of the extratropical transition of Floyd (1999): Structural evolution and responsible mechanisms for the heavy rainfall over the northeast United States. *Mon. Wea. Rev.*, **131**, 2905–2926, doi:10.1175/1520-0493(2003)131<2905:NSOTET>2.0.CO;2.
- , F. Buonaiuto, M. J. Bowman, R. E. Wilson, R. Flood, R. Hunter, A. Mintz, and D. Hill, 2008: New York City's vulnerability to coastal flooding. *Bull. Amer. Meteor. Soc.*, **89**, 829–841, doi:10.1175/2007BAMS2401.1.
- , Z. Zhang, K. A. Lombardo, E. Chang, P. Liu, and M. Zhang, 2013: Historical evaluation and future prediction of eastern North American and western Atlantic extratropical cyclones in the CMIP5 models during the cool season. *J. Climate*, **26**, 6882–6903, doi:10.1175/JCLI-D-12-00498.1.
- , and Coauthors, 2015: Exploring water level sensitivity for metropolitan New York during Sandy (2012) using ensemble storm surge simulations. *J. Mar. Sci. Eng.*, **3**, 428–443, doi:10.3390/jmse3020428.
- Donner, L. J., and Coauthors, 2011: The dynamical core, physical parameterizations, and basic simulation characteristics of the atmospheric component AM3 of the GFDL global coupled model CM3. *J. Climate*, **24**, 3484–3519, doi:10.1175/2011JCLI3955.1.
- Dufresne, J.-L., and Coauthors, 2013: Climate change projections using the IPSL-CM5 Earth System Model: From CMIP3 to CMIP5. *Climate Dyn.*, **40**, 2123–2165, doi:10.1007/s00382-012-1636-1.
- Durran, D. R., and J. B. Klemp, 1982: On the effects of moisture on the Brunt-Väisälä frequency. *J. Atmos. Sci.*, **39**, 2152–2158, doi:10.1175/1520-0469(1982)039<2152:OTEOMO>2.0.CO;2.
- Emanuel, K. A., M. Fantini, and A. J. Thorpe, 1987: Baroclinic instability in an environment of small stability to slantwise moist convection. Part I: Two-dimensional models. *J. Atmos. Sci.*, **44**, 1559–1573, doi:10.1175/1520-0469(1987)044<1559:BIIAEO>2.0.CO;2.
- Emori, S., and S. J. Brown, 2005: Dynamic and thermodynamic changes in mean and extreme precipitation under changed climate. *Geophys. Res. Lett.*, **32**, L17706, doi:10.1029/2005GL023272.
- Field, P. R., and R. Wood, 2007: Precipitation and cloud structure in midlatitude cyclones. *J. Climate*, **20**, 233–254, doi:10.1175/JCLI3998.1.
- Frierson, D. M., 2006: Robust increases in midlatitude static stability in simulations of global warming. *Geophys. Res. Lett.*, **33**, L24816, doi:10.1029/2006GL027504.
- Gent, P. R., and Coauthors, 2011: The Community Climate System Model version 4. *J. Climate*, **24**, 4973–4991, doi:10.1175/2011JCLI4083.1.
- Hawcroft, M. K., L. C. Shaffrey, K. I. Hodges, and H. F. Dacre, 2012: How much Northern Hemisphere precipitation is associated with extratropical cyclones? *Geophys. Res. Lett.*, **39**, L24809, doi:10.1029/2012GL053866.
- , —, —, and —, 2016: Can climate models represent the precipitation associated with extratropical cyclones? *Climate Dyn.*, **47**, 679–695, doi:10.1007/s00382-015-2863-z.
- Held, I. M., and B. J. Soden, 2006: Robust responses of the hydrological cycle to global warming. *J. Climate*, **19**, 5686–5699, doi:10.1175/JCLI3990.1.
- Hodges, K. I., 1994: A general method for tracking analysis and its application to meteorological data. *Mon. Wea. Rev.*, **122**, 2573–2586, doi:10.1175/1520-0493(1994)122<2573:AGMFTA>2.0.CO;2.
- , 1995: Feature tracking on the unit sphere. *Mon. Wea. Rev.*, **123**, 3458–3465, doi:10.1175/1520-0493(1995)123<3458:FTOTUS>2.0.CO;2.
- Jiang, Q., and J. D. Doyle, 2009: The impact of moisture on mountain waves during T-REX. *Mon. Wea. Rev.*, **137**, 3888–3906, doi:10.1175/2009MWR2985.1.
- Jones, C. D., and Coauthors, 2011: The HadGEM2-ES implementation of CMIP5 centennial simulations. *Geosci. Model Dev.*, **4**, 543–570, doi:10.5194/gmd-4-543-2011.
- Knutti, R., and J. Sedláček, 2013: Robustness and uncertainties in the new CMIP5 climate model projections. *Nat. Climate Change*, **3**, 369–373, doi:10.1038/nclimate1716.
- Lackmann, G. M., 2002: Potential vorticity redistribution, the low-level jet, and moisture transport in extratropical cyclones. *Mon. Wea. Rev.*, **130**, 59–74, doi:10.1175/1520-0493(2002)130<0059:CFPVMT>2.0.CO;2.

- , and J. R. Gyakum, 1999: Heavy cold-season precipitation in the northwestern United States: Synoptic climatology and an analysis of the flood of 17–18 January 1986. *Wea. Forecasting*, **14**, 687–700, doi:10.1175/1520-0434(1999)014<0687:HCSFIT>2.0.CO;2.
- Lau, W. K. M., H. T. Wu, and K. M. Kim, 2013: A canonical response of precipitation characteristics to global warming from CMIP5 models. *Geophys. Res. Lett.*, **40**, 3163–3169, doi:10.1002/grl.50420.
- Lombardo, K., B. A. Colle, and Z. Zhang, 2015: Evaluation of historical and future cool season precipitation over the eastern United States and western Atlantic storm track using CMIP5 models. *J. Climate*, **28**, 451–467, doi:10.1175/JCLI-D-14-00343.1.
- Maloney, E. D., and Coauthors, 2014: North American climate in CMIP5 experiments: Part III: Assessment of twenty-first-century projections. *J. Climate*, **27**, 2230–2270, doi:10.1175/JCLI-D-13-00273.1.
- Marciano, C. G., G. M. Lackmann, and W. A. Robinson, 2015: Changes in U.S. East Coast cyclone dynamics with climate change. *J. Climate*, **28**, 468–484, doi:10.1175/JCLI-D-14-00418.1.
- Michou, M., and Coauthors, 2011: A new version of the CNRM Chemistry-Climate Model, CNRM-CCM: Description and improvements from the CCMVal-2 simulations. *Geosci. Model Dev.*, **4**, 873–900, doi:10.5194/gmd-4-873-2011.
- Naud, C. M., D. J. Posselt, and S. C. Van Den Heever, 2012: Observational analysis of cloud and precipitation in midlatitude cyclones: Northern versus Southern Hemisphere warm fronts. *J. Climate*, **25**, 5135–5151, doi:10.1175/JCLI-D-11-00569.1.
- , J. F. Booth, D. J. Posselt, and S. C. Heever, 2013: Multiple satellite observations of cloud cover in extratropical cyclones. *J. Geophys. Res. Atmos.*, **118**, 9982–9996, doi:10.1002/jgrd.50718.
- Novak, D. R., B. A. Colle, and S. E. Yuter, 2008: High-resolution observations and model simulations of the life cycle of an intense mesoscale snowband over the northeastern United States. *Mon. Wea. Rev.*, **136**, 1433–1456, doi:10.1175/2007MWR2233.1.
- O’Gorman, P. A., R. P. Allan, M. P. Byrne, and M. Previdi, 2012: Energetic constraints on precipitation under climate change. *Surv. Geophys.*, **33**, 585–608, doi:10.1007/s10712-011-9159-6.
- Pfahl, S., and M. Sprenger, 2016: On the relationship between extratropical cyclone precipitation and intensity. *Geophys. Res. Lett.*, **43**, 1752–1758, doi:10.1002/2016GL068018.
- Picca, J. C., D. M. Schultz, B. A. Colle, S. Ganetis, D. R. Novak, and M. J. Sienkiewicz, 2014: The value of dual-polarization radar in diagnosing the complex microphysical evolution of an intense snowband. *Bull. Amer. Meteor. Soc.*, **95**, 1825–1834, doi:10.1175/BAMS-D-13-00258.1.
- Scoccimarro, E., S. Gualdi, A. Bellucci, M. Zampieri, and A. Navarra, 2013: Heavy precipitation events in a warmer climate: Results from CMIP5 models. *J. Climate*, **26**, 7902–7911, doi:10.1175/JCLI-D-12-00850.1.
- Seager, R., N. Naik, and G. A. Vecchi, 2010: Thermodynamic and dynamic mechanisms for large-scale changes in the hydrological cycle in response to global warming. *J. Climate*, **23**, 4651–4668, doi:10.1175/2010JCLI3655.1.
- Stephens, G. L., and T. D. Ellis, 2008: Controls of global-mean precipitation increases in global warming GCM experiments. *J. Climate*, **21**, 6141–6155, doi:10.1175/2008JCLI2144.1.
- Tamarin, T., and Y. Kaspi, 2016: The poleward motion of extratropical cyclones from a potential vorticity tendency analysis. *J. Atmos. Sci.*, **73**, 1687–1707, doi:10.1175/JAS-D-15-0168.1.
- Taylor, K. E., R. J. Stouffer, and G. A. Meehl, 2012: An overview of CMIP5 and the experiment design. *Bull. Amer. Meteor. Soc.*, **93**, 485–498, doi:10.1175/BAMS-D-11-00094.1.
- Trenberth, K. E., 2011: Changes in precipitation with climate change. *Climate Res.*, **47**, 123–138, doi:10.3354/cr00953.
- Vecchi, G. A., and B. J. Soden, 2007: Global warming and the weakening of the tropical circulation. *J. Climate*, **20**, 4316–4340, doi:10.1175/JCLI4258.1.
- Volodin, E. M., N. A. Dianskii, and A. V. Gusev, 2010: Simulating present-day climate with the INMCM4.0 Coupled Model of the Atmospheric and Oceanic General Circulations. *Izv. Atmos. Oceanic Phys.*, **46**, 414–431, doi:10.1134/S000143381004002X.
- Watanabe, S., and Coauthors, 2011: MIROC-ESM: Model description and basic results of CMIP5-20c3m experiments. *Geosci. Model Dev.*, **4**, 845–872, doi:10.5194/gmd-4-845-2011.
- Watterson, I. G., 2006: The intensity of precipitation during extratropical cyclones in global warming simulations: A link to cyclone intensity? *Tellus*, **58A**, 82–97, doi:10.1111/j.1600-0870.2006.00147.x.
- Willison, J., W. A. Robinson, and G. M. Lackmann, 2013: The importance of resolving mesoscale latent heating in the North Atlantic storm track. *J. Atmos. Sci.*, **70**, 2234–2250, doi:10.1175/JAS-D-12-0226.1.
- Xie, P., and P. A. Arkin, 1997: Global precipitation: A 17-year monthly analysis based on gauge observations, satellite estimates, and numerical model outputs. *Bull. Amer. Meteor. Soc.*, **78**, 2539–2558, doi:10.1175/1520-0477(1997)078<2539:GPAYMA>2.0.CO;2.
- Yukimoto, S., and Coauthors, 2012: A new global climate model of the Meteorological Research Institute: MRI-CGCM3—Model description and basic performance. *J. Meteor. Soc. Japan*, **90A**, 23–64, doi:10.2151/jmsj.2012-A02.
- Zanchettin, D., A. Rubino, D. Matei, O. Bothe, and J. H. Jungclauss, 2013: Multidecadal-to-centennial SST variability in the MPI-ESM simulation ensemble for the last millennium. *Climate Dyn.*, **40**, 1301–1318, doi:10.1007/s00382-012-1361-9.
- Zappa, G., L. C. Shaffrey, K. I. Hodges, P. G. Sansom, and D. B. Stephenson, 2013: A multimodel assessment of future projections of North Atlantic and European extratropical cyclones in the CMIP5 climate models. *J. Climate*, **26**, 5846–5862, doi:10.1175/JCLI-D-12-00573.1.